

# How robust can we identify and quantify stellar bars using JWST observations?

Reporter: Xinyue Liang (梁馨月)

Supervisors: Dr. Si-yue Yu, Prof. Taotao Fang, and Prof. Luis C. Ho,

# Background

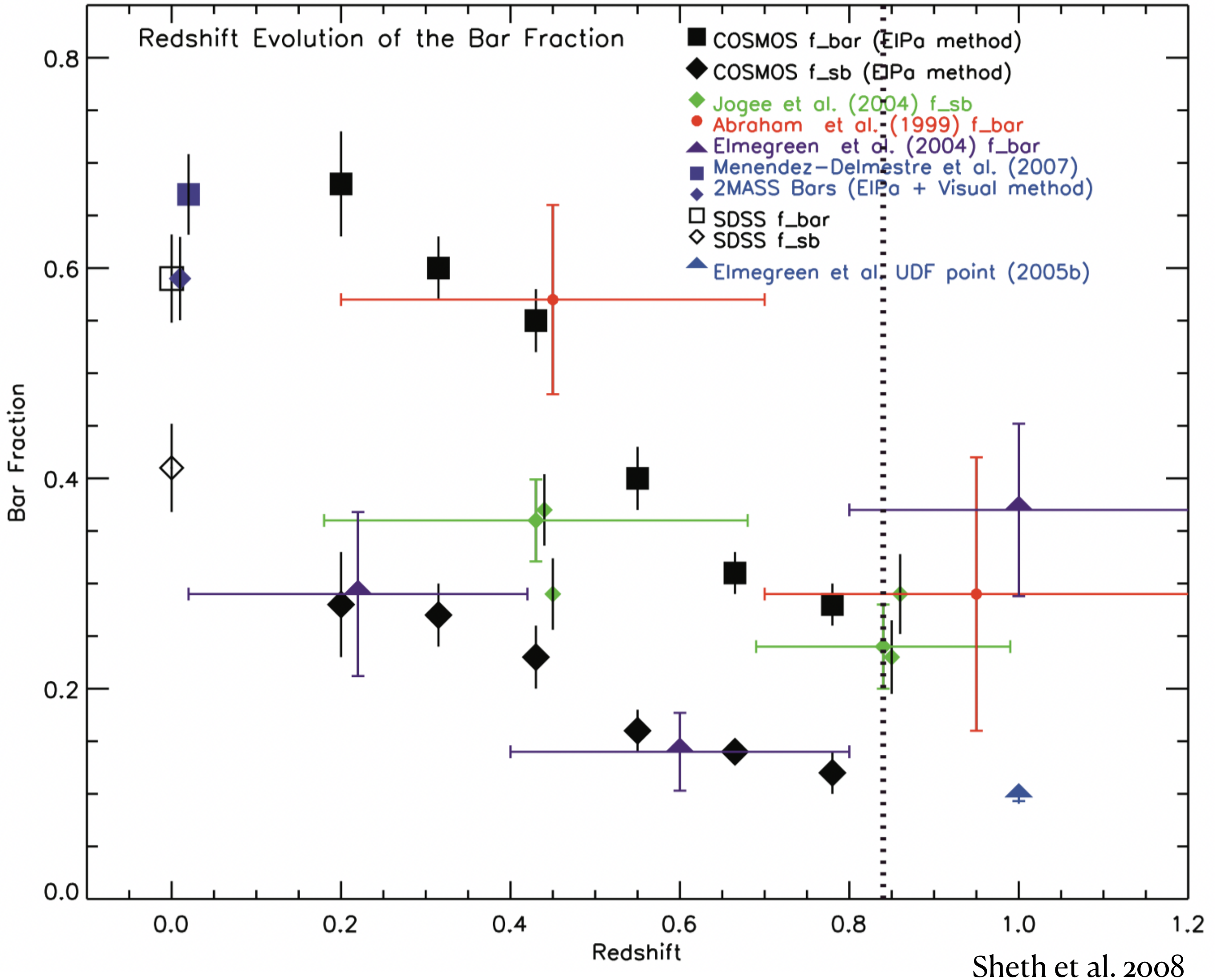
- In local Universe, there are ~ 60% of disk galaxies hosting a bar when viewed both in optical and near-infrared (NIR) wavelengths.
- It is generally accepted that stellar bars play an important role in galaxy evolution. The non-axisymmetric bar gravitational potential drives cold gas flow toward the galaxy center, enhancing central star formation and leading to the growth of pseudo bulges.



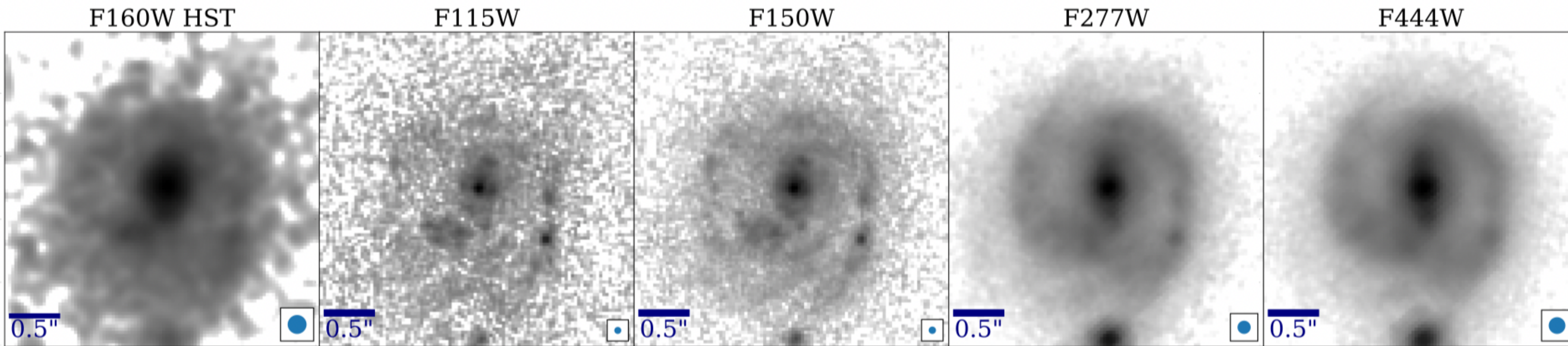
NGC1300

# Background

- Through observations from the *Hubble Space Telescope* (HST), the bar fraction is found to evolve with redshift.
- Results on how the bar fraction varies out to  $z \sim 1$  have been mixed.
- Identifying and quantifying bar structures at high redshift using HST observations present a considerable challenge.



# Background

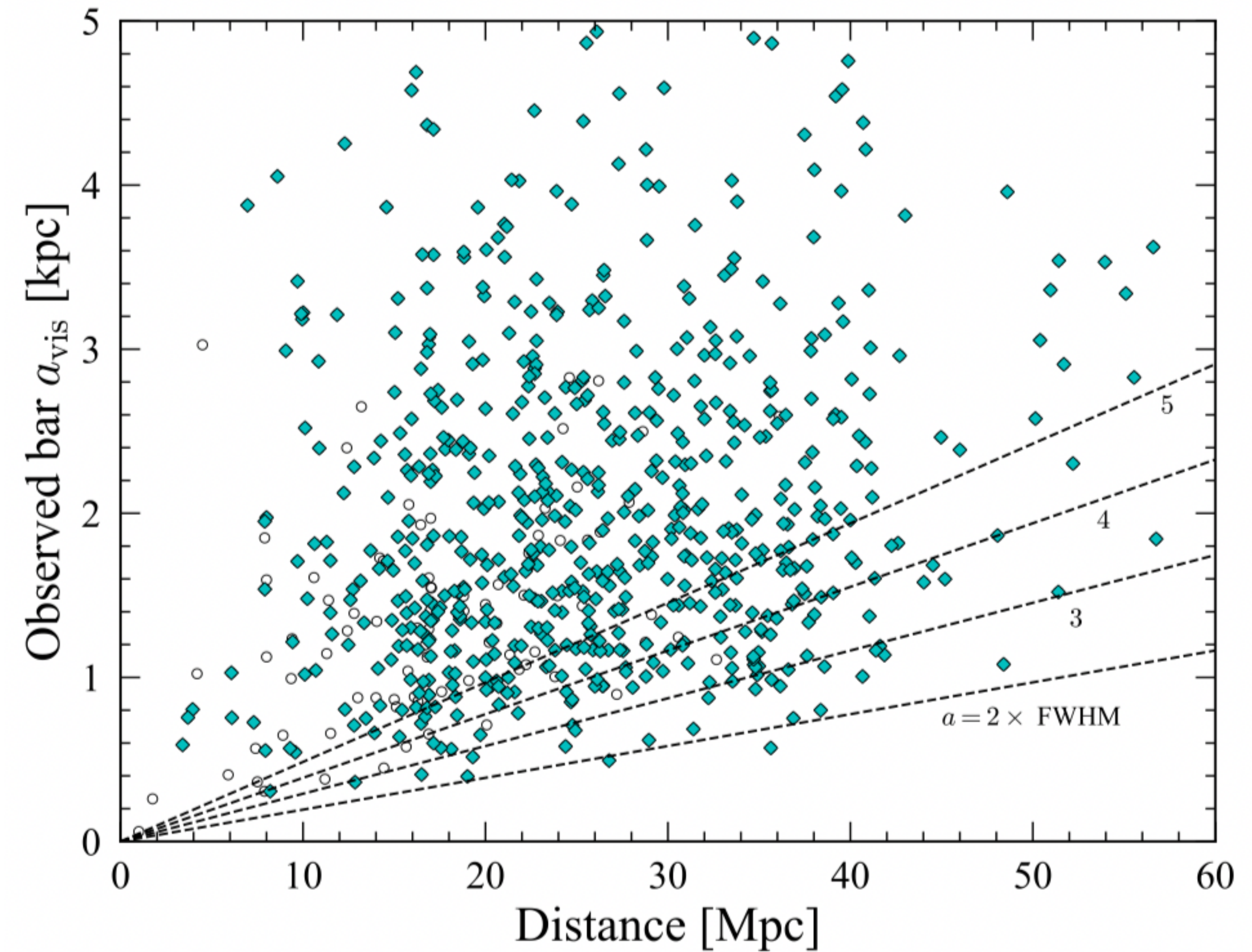


Guo et al. 2022

- The Hubble Sequence was already established by  $z \approx 6$ . Remarkably, barred galaxies at  $z \approx 2$ , previously undetected in HST observations, have now been identified using JWST.
- While JWST imaging offers better physical resolution in the NIR compared to HST, it still falls short of the physical resolution achievable in ground-based observations of nearby galaxies.
-

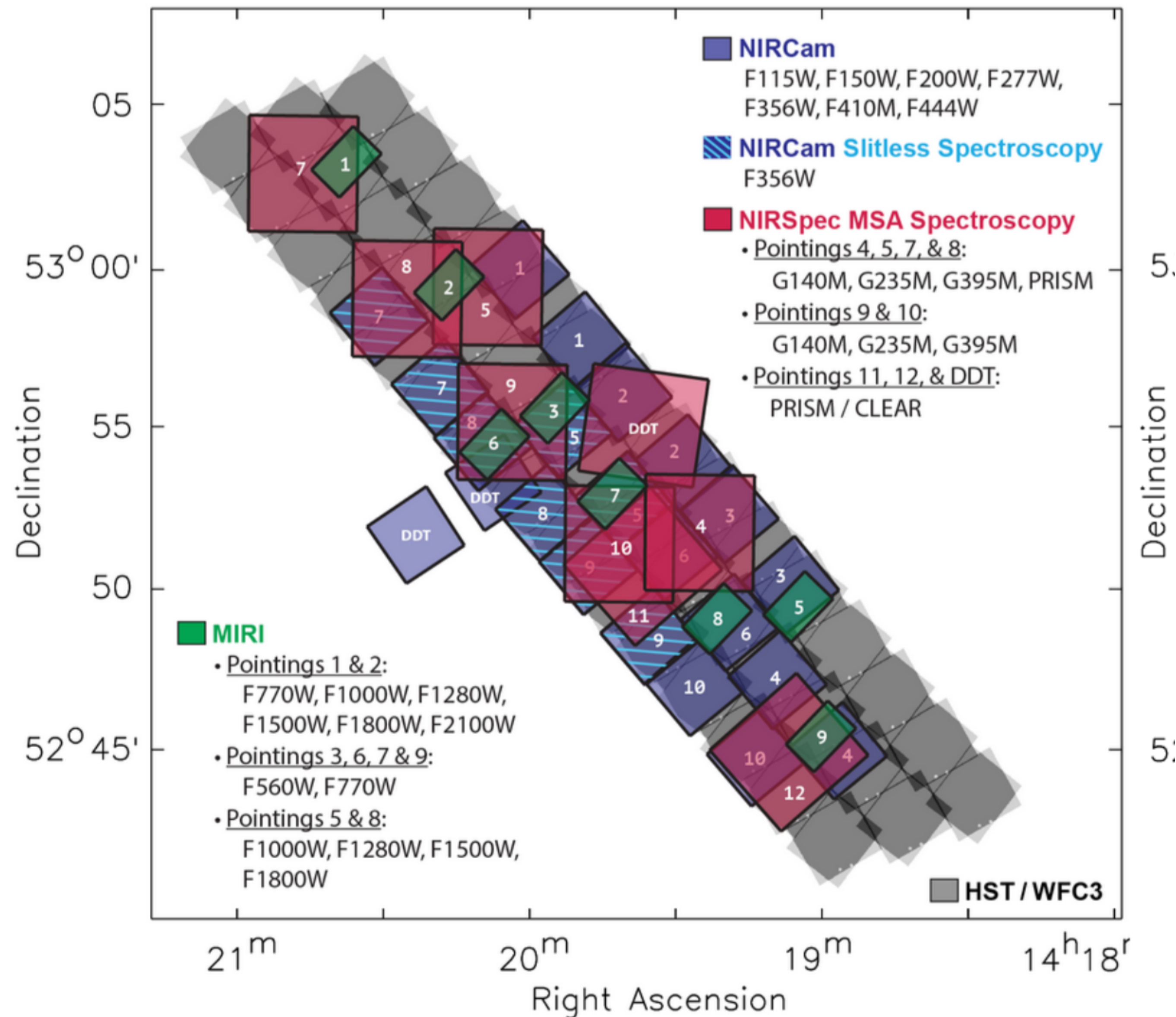
# Background

- By analysing projected bar radius in galaxies from the Spitzer Survey of Stellar Structure in Galaxies, Erwin (2018) showed that most of the projected bar radius are larger than  $2 \times \text{FWHM}$  and thus suggested this value as the detection limit for projected bar radius.
- Nevertheless, these detection limits for bar radius have not yet been validated in a quantitative way, especially under typical JWST observational conditions.



# CEERS

- CEERS is an early release science surveys in Cycle 1, covering the Extended Growth Strip field (EGS) of the Cosmic Assembly Near-IR Deep Extragalactic Legacy Survey (CANDELS).
- The complete program involves ten pointings with Near-Infrared Camera short and long-wavelength channels, covering a total of 100 sq. arcmin. Each pointing was observed with seven filters.



# Motivation

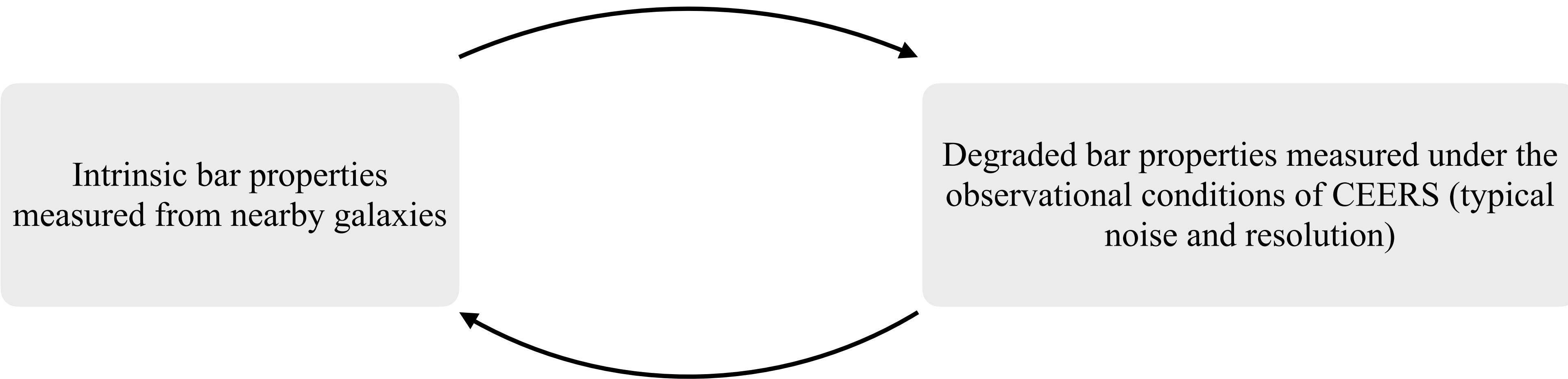
- Resolution may also impact measured bar properties, such as length, ellipticity, and position angle, which are frequently employed to study the formation and evolution of bars.
- The launch of JWST enable us to detect barred galaxies in the early Universe. However, it is challenging to interpret the observation results without knowing the systematic bias caused by the limit of observation.
- 

# Goal

- We aim to understand how the observational factors can influence the identification and quantification of bars, and to develop methods to restore the degraded bar properties to their intrinsic values.

# Core Idea

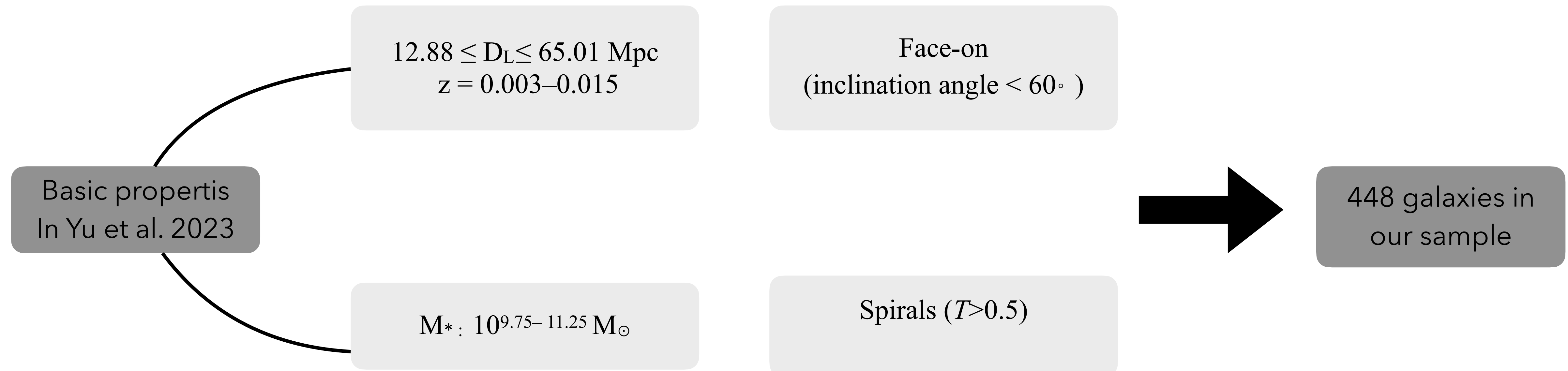
**This work:** Image simulation & re-measurements



**Future work:** correct the measurement bias to obtain intrinsic properties

# Observational material

- We take advantage of the sample of nearby galaxies defined by Yu et al. (2023), which is constructed from the Siena Galaxy Atlas (SGA). SGA is based on the Dark Energy Spectroscopic Instrument (DESI) Legacy Imaging Surveys.



# Classification process

- We adopt **ellipse fitting method** to identify bars and measure their associated properties. Unlike the traditional ellipse fitting method that automatically identifies bars through the signatures of position angle (PA) profile and ellipticity ( $\epsilon$ ) profile, we take a different route.
- We save the properties of barred galaxies, including  $\epsilon_{\text{bar}}$ ,  $\text{PA}_{\text{bar}}$ , and the projected bar size represented as semi-major axis ( $a_{\text{bar}}$ ).
- Finally, 304 out of 448 spiral galaxies are classified as barred galaxies, resulting 68% bar fraction, which is consistent with previous studies that visually identified bars in both optical and NIR images.

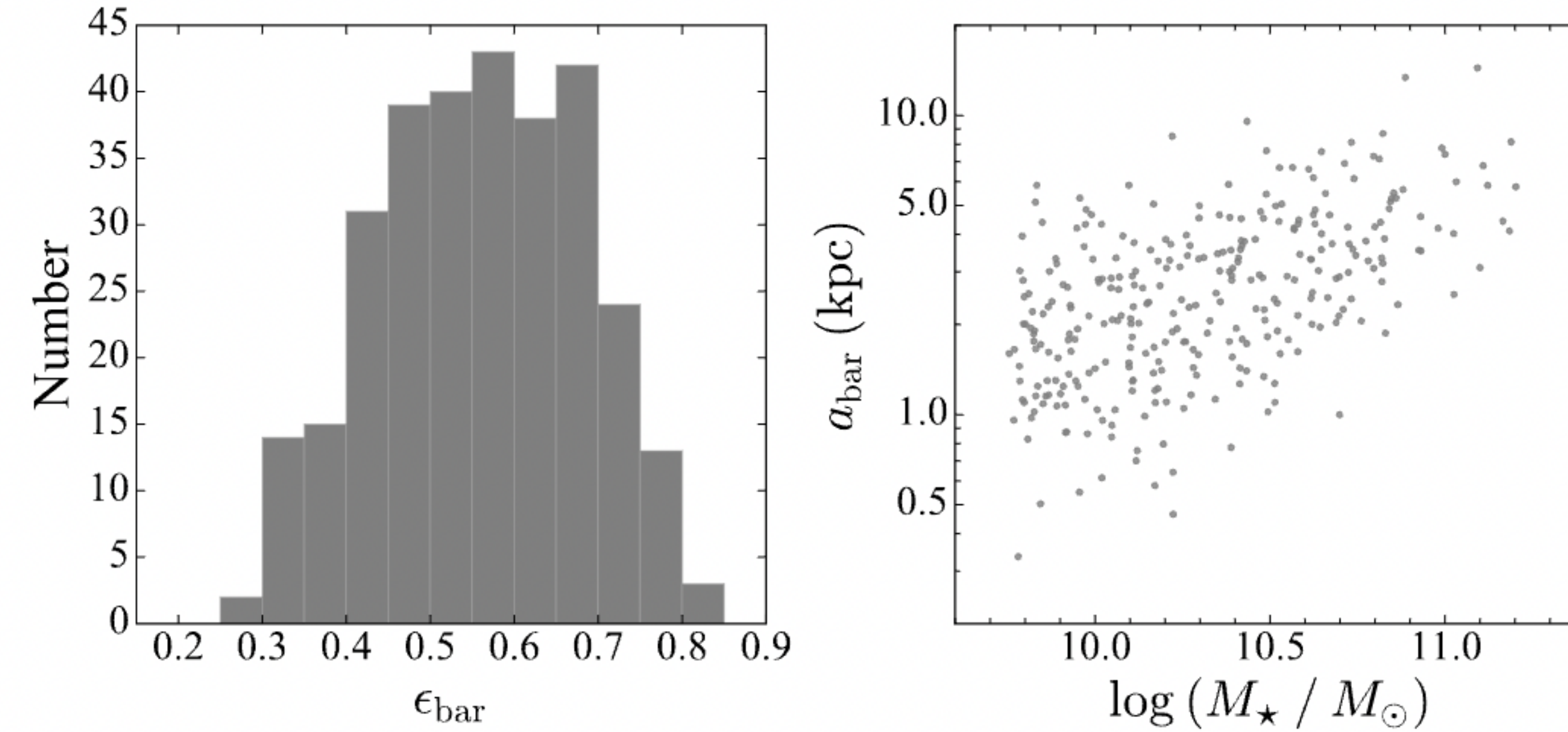
Run **ellipse** for each galaxy

Identify bar candidates by observing a local maximum in their  $\epsilon$  profile greater than 0.1, or a decrease of at least 0.05.

Mark one of the candidates on the image, then visually check whether it accurately represents a bar.

If one of candidates is confirmed as a bar, the galaxy is classified as barred. Otherwise, it is classified as unbarred.

# Basic properties of barred galaxies



- Our sample covers a wide range of bars, with  $\epsilon_{\text{bar}}$  values spanning from 0.2 to 0.8 and  $a_{\text{bar}}$  ranging from 0.3 to 10 kpc.
- Furthermore, among galaxies with stellar masses ( $M_{\star}$ ) ranging from  $10^{9.75-11.25} M_{\odot}$  in our sample, we observe a correlation between  $a_{\text{bar}}$  and  $M_{\star}$ .

# Image simulations

## Low-resolution images

DESI images

Rescale the original barred galaxy images to  
match the  $\alpha_{\text{bar}}$  with  $N$  times the FWHM

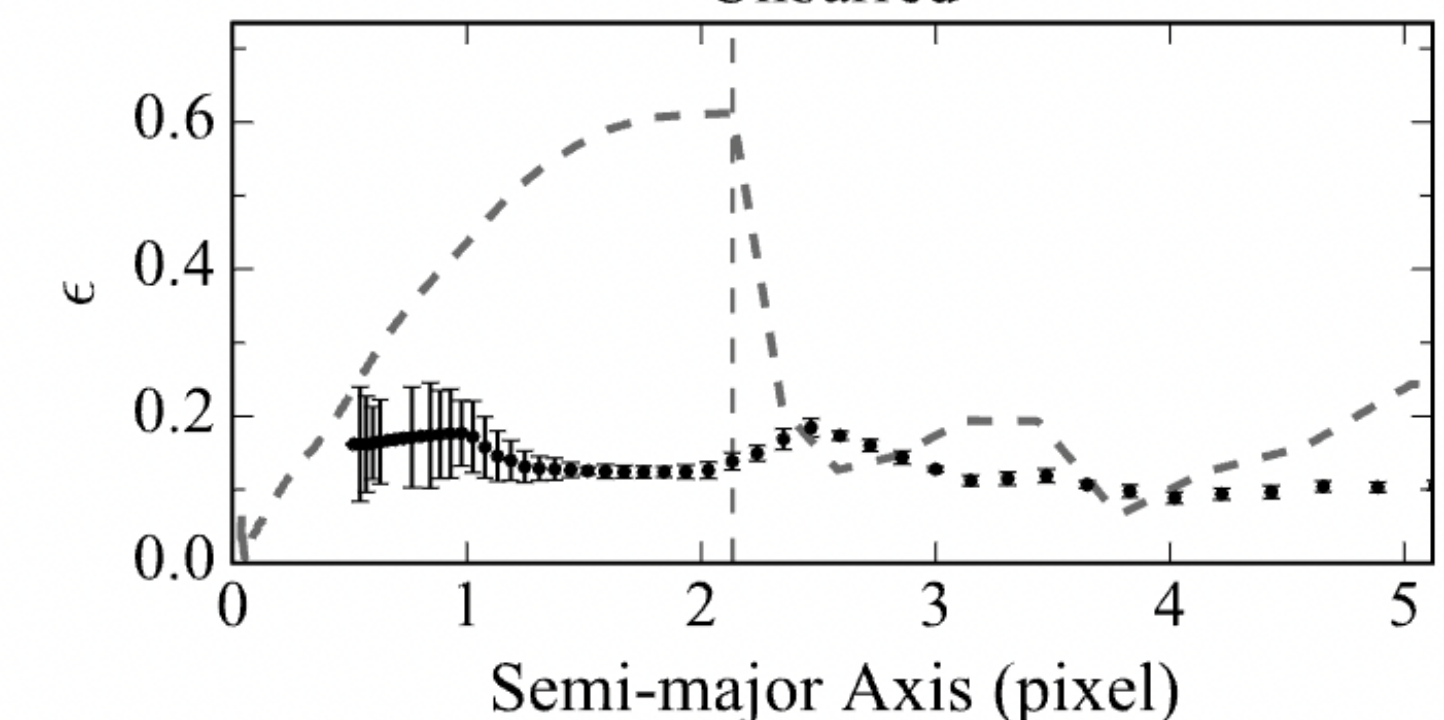
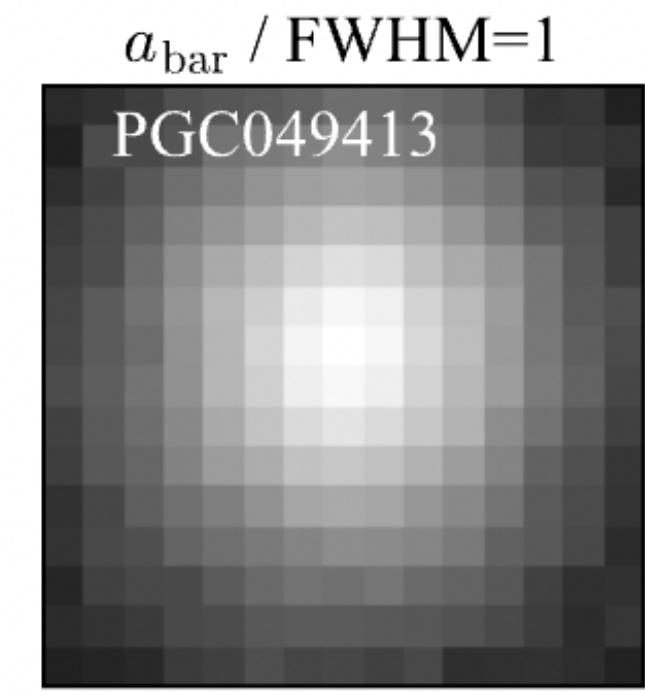
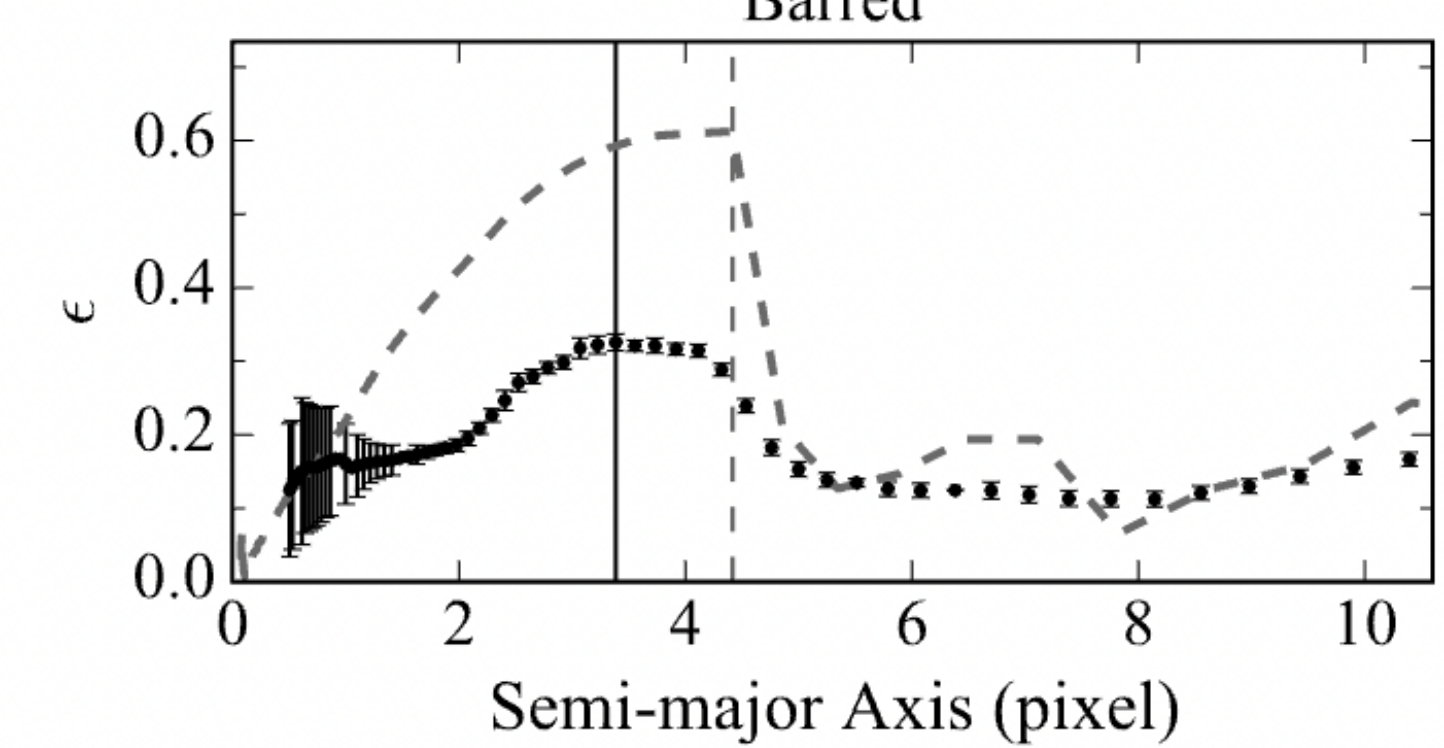
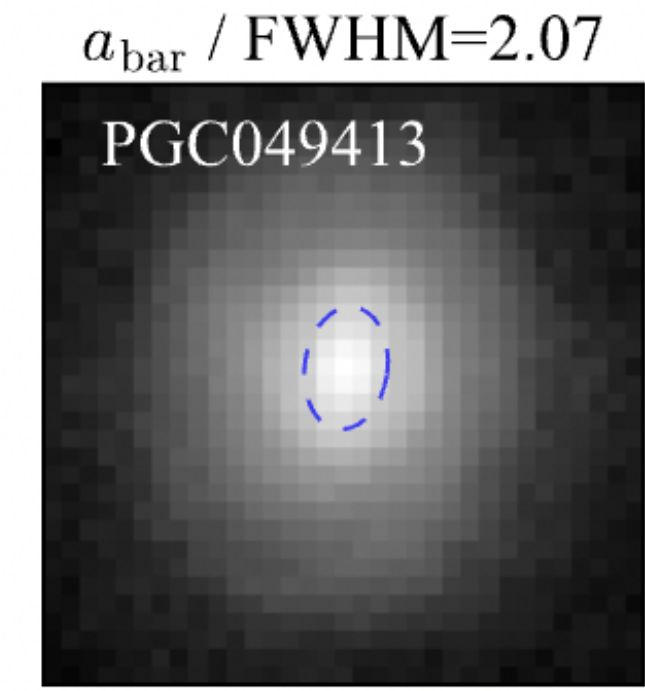
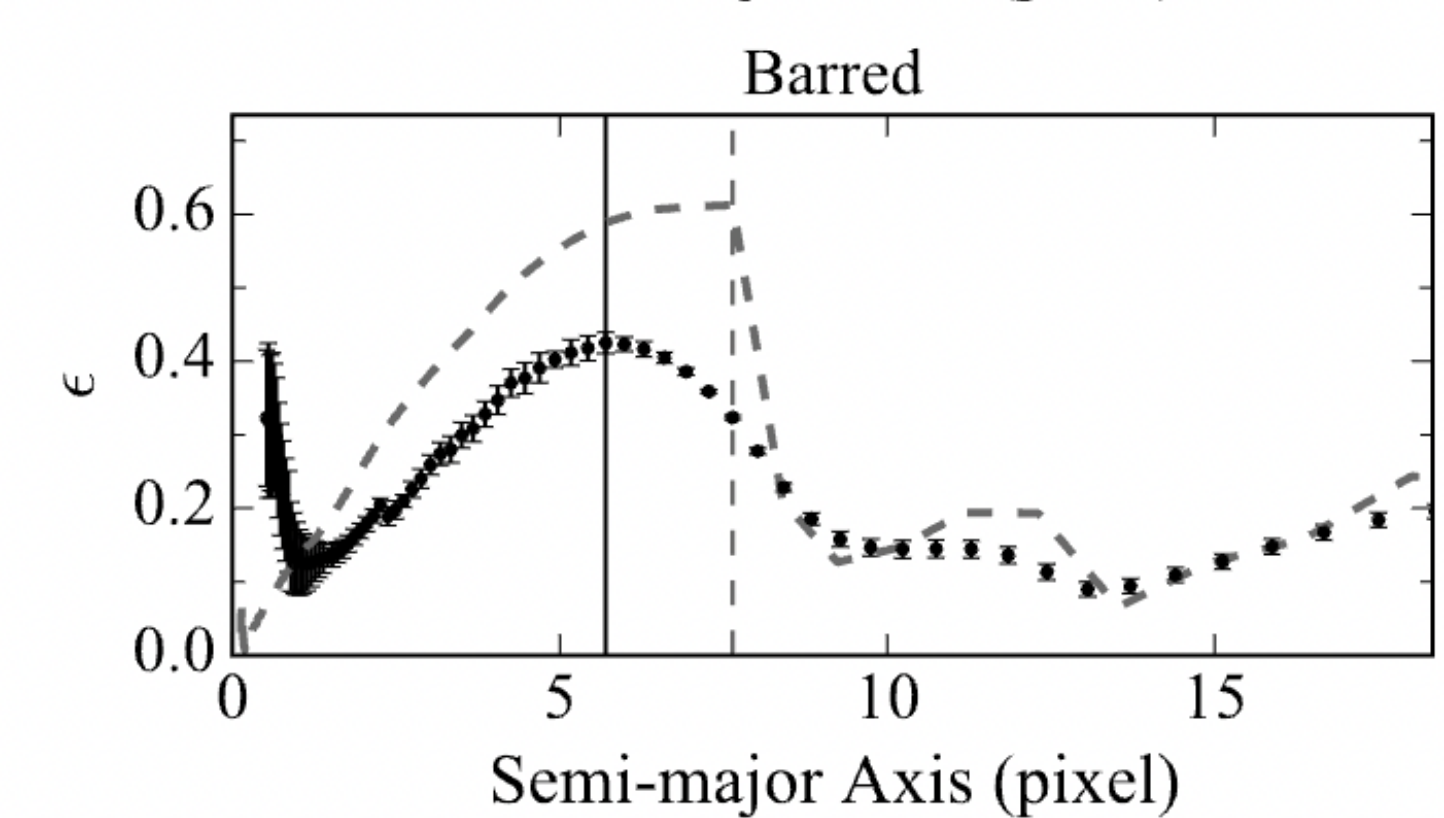
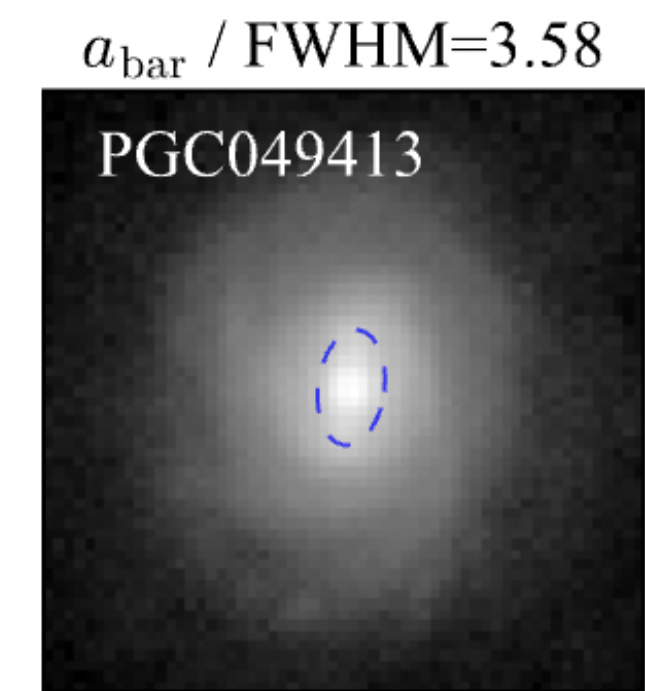
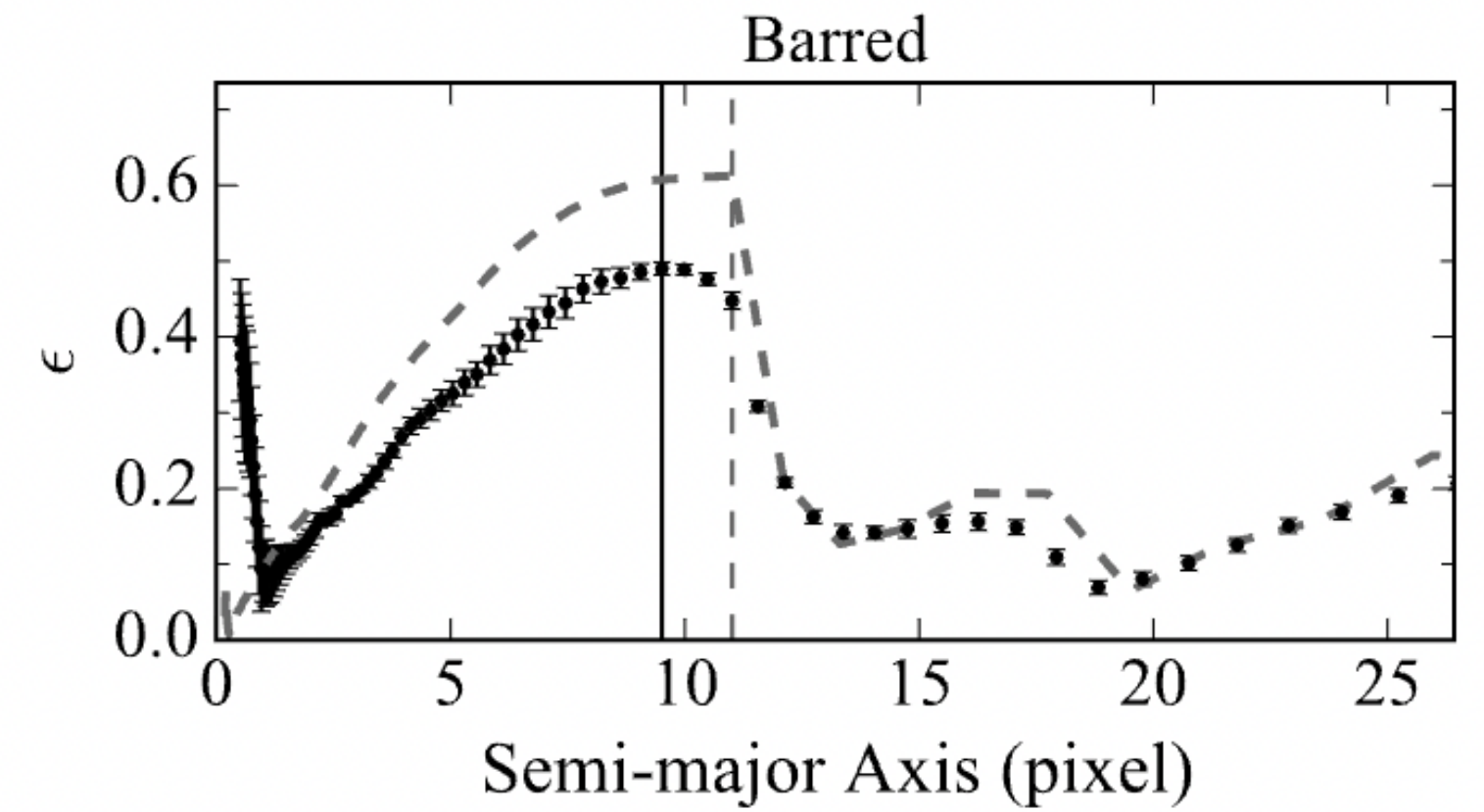
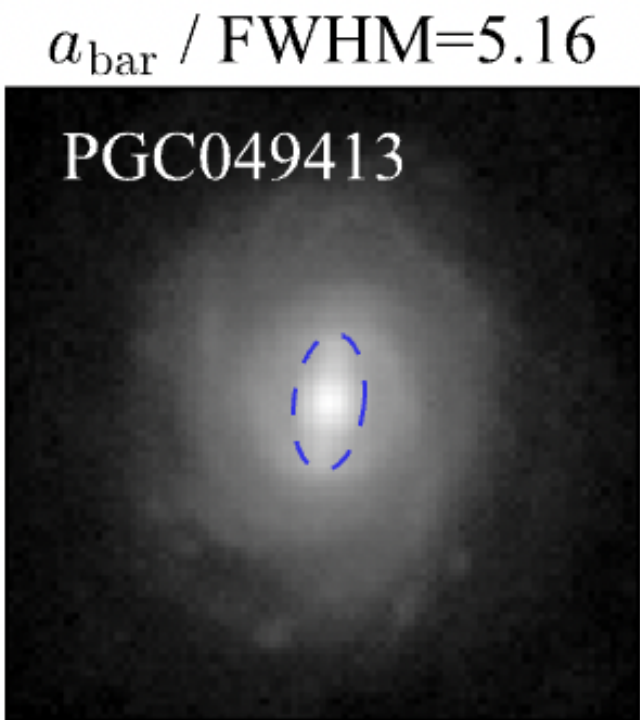
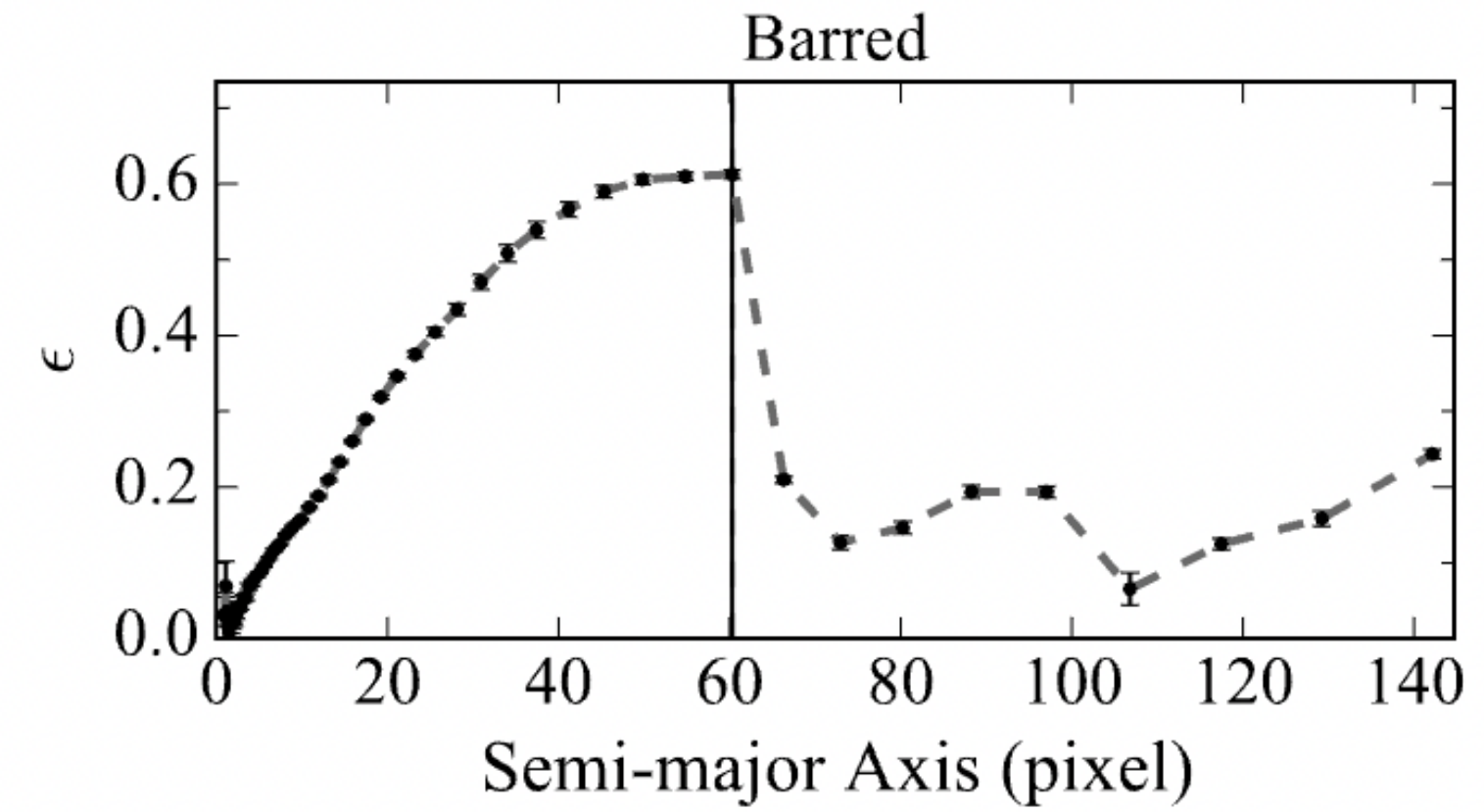
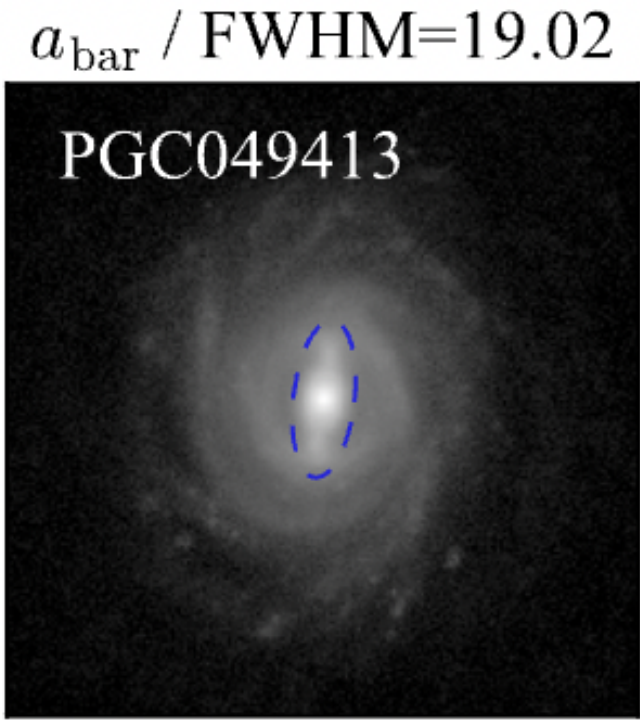


$N = 1.0, 1.2, 1.44, 1.73, 2.07, 2.49, 2.99, 3.58,$   
 $4.3, 5.16, \text{ and } 10$

Low- resolution images  
( $N$ -times-FWHM images)

- In addition, to simulate galaxies in a similar rest-frame optical wavelength, we will employ the F115W for  $0.75 \leq z < 1.0$ , the F150W for  $1.0 \leq z < 2.0$ , and the F200W for  $2.0 \leq z < 3.0$ .
- The FWHM of F115W, F150W, and F200W PSF is 0.037, 0.049, and 0.064 arcsec, respectively.
- The properties measured from low-resolution images are denoted as  $\epsilon_N$ ,  $a_N$  and  $\text{PA}_N$

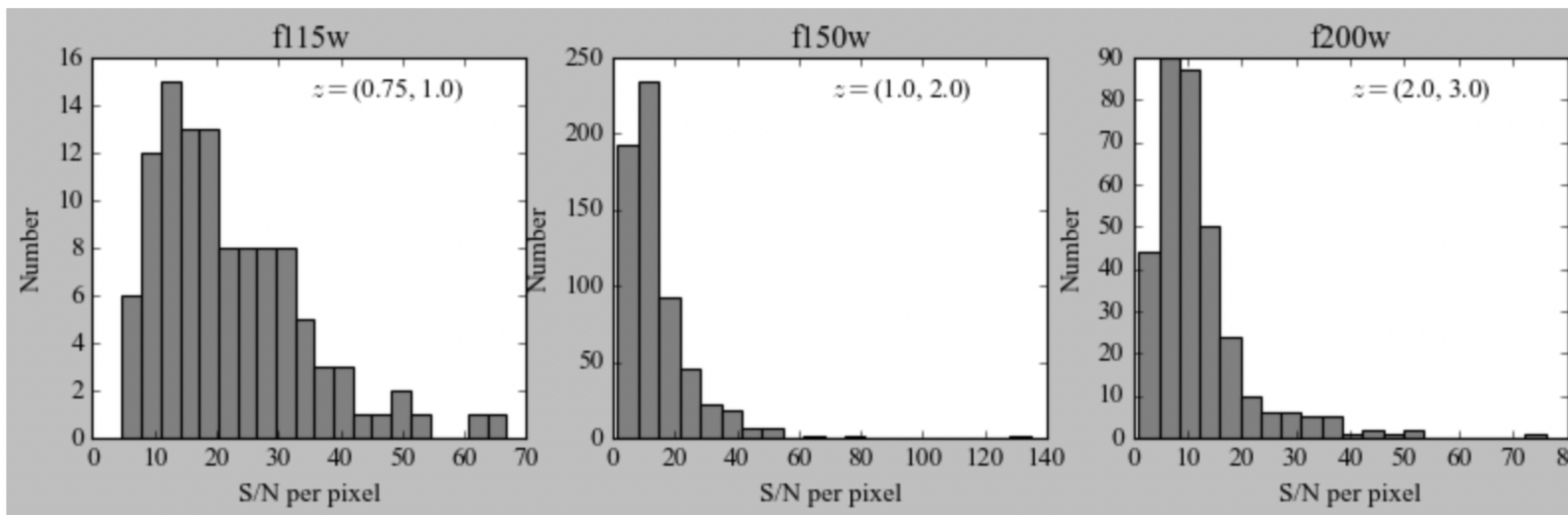
# Low-resolution images



- Black solid vertical line — bar re-measured from the image.
- Grey dashed vertical line — bar measured from DESI image
- Grey dashed curve — rescaled  $\epsilon$  profile of DESI image

# Image simulations

## Low-S/N images



- We calculate the median S/N for galaxies observed with each filter within its corresponding redshift range, yielding values of 19.28, 10.92, and 9.76 for F115W, F150W, and F200W, respectively.
- The properties measured from low-S/N images are denoted as  $\epsilon_{S/N}$ ,  $\alpha_{S/N}$  and  $PA_{S/N}$

4.3-times- FWHM  
images

Rescale the 4.3-times-FWHM images flux and  
to match various levels of S/N



S/N = 3, 4.2, 5.9, 8.2, 11.5, 16.1, 22.6, 31.6, 44.3, 62

Low- S/N images

# Low-S/N images

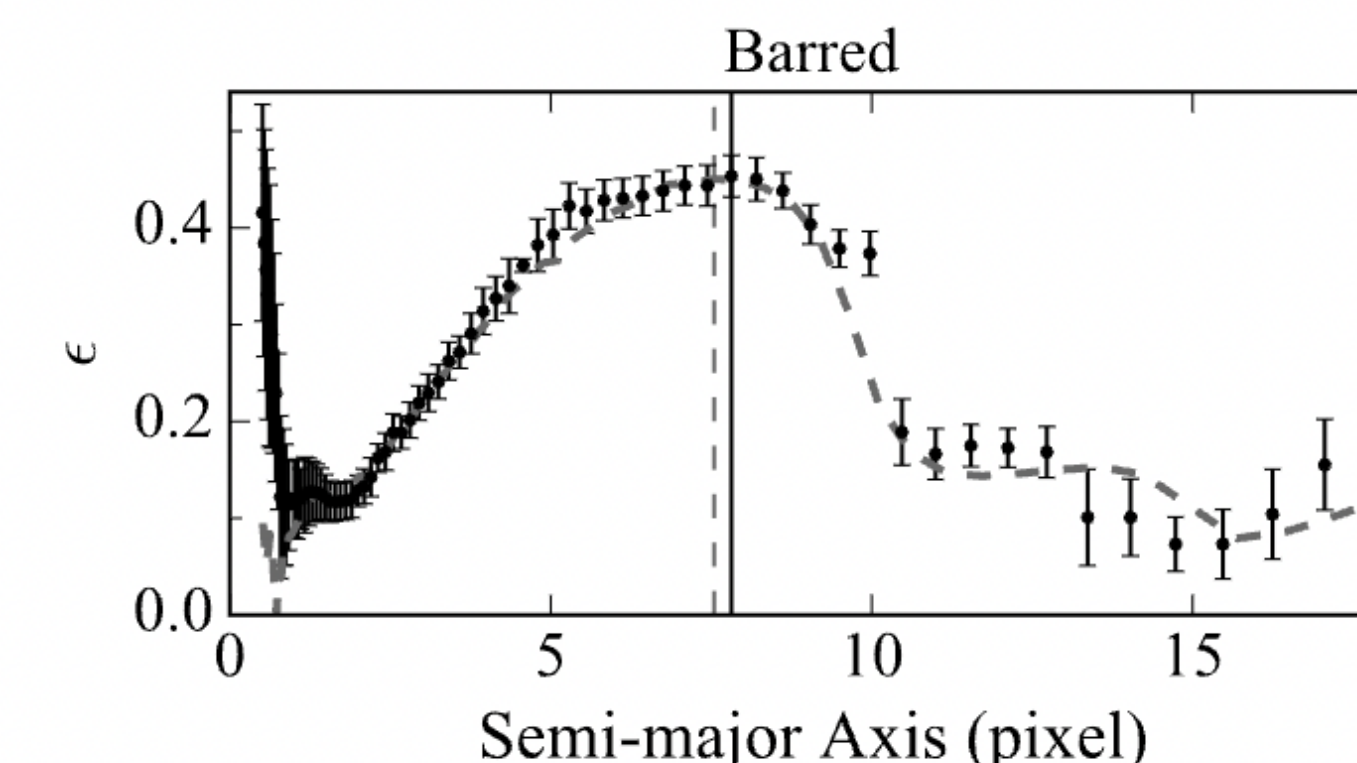
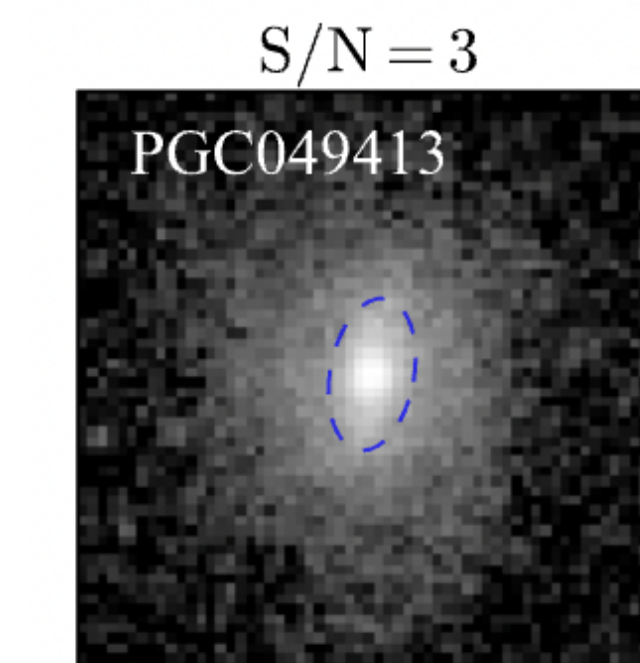
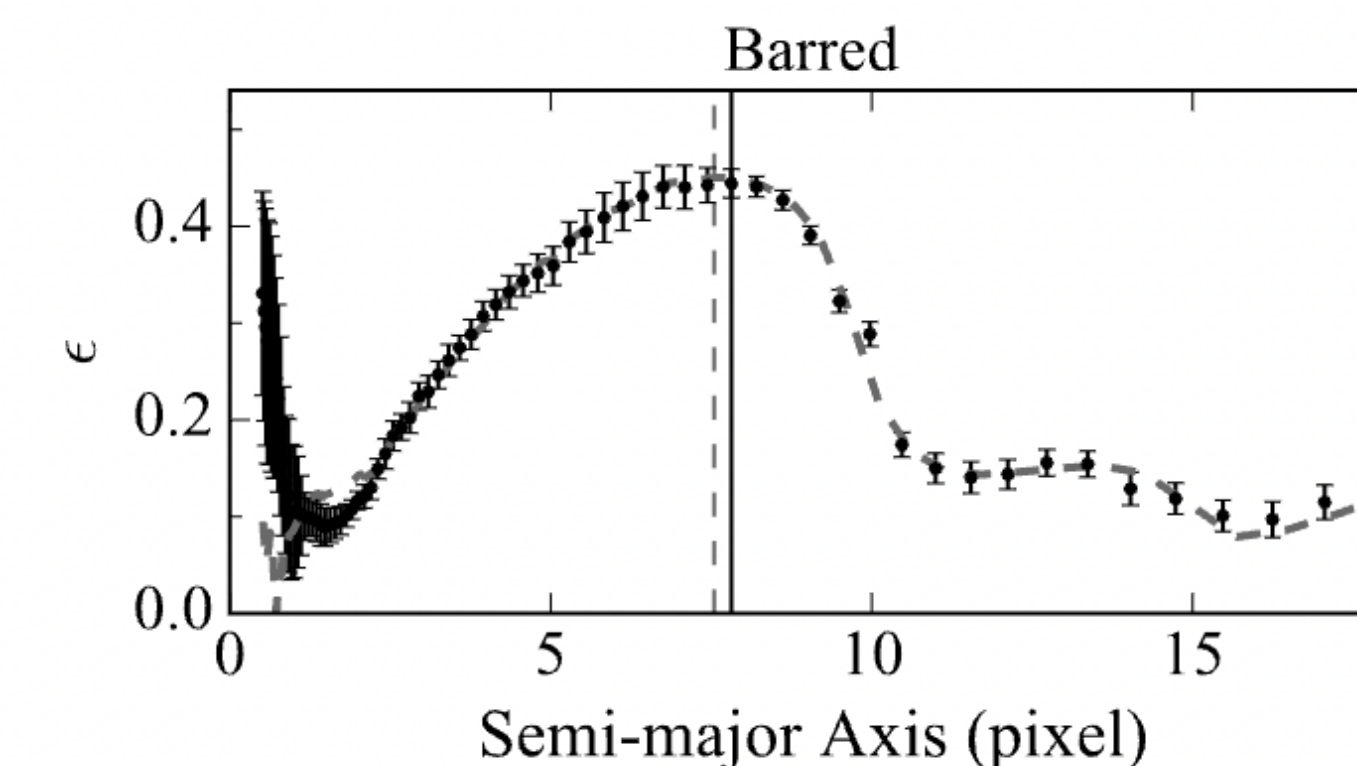
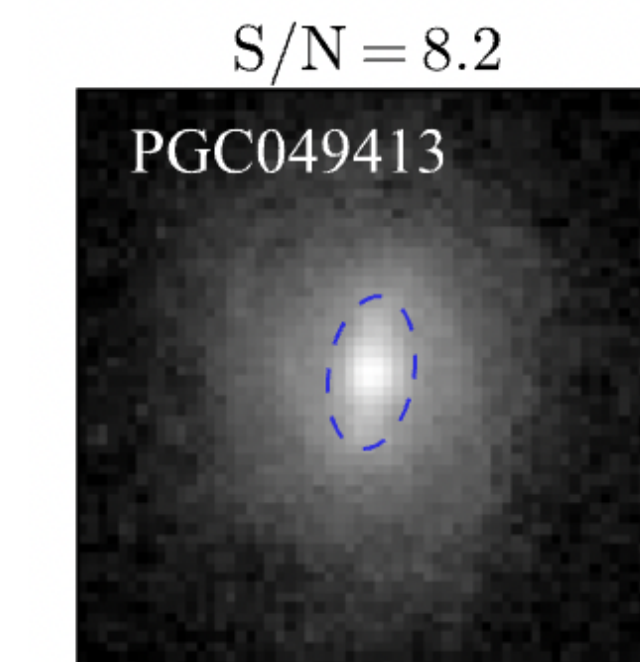
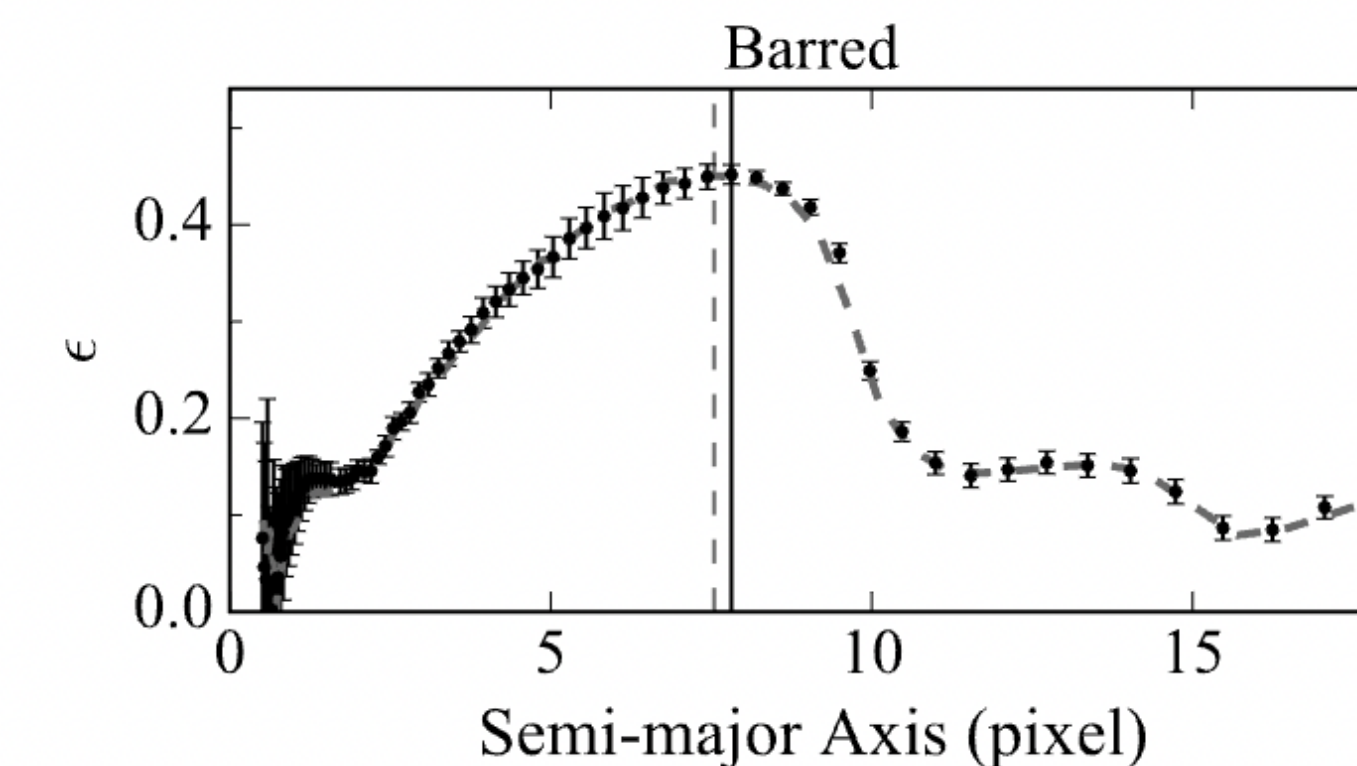
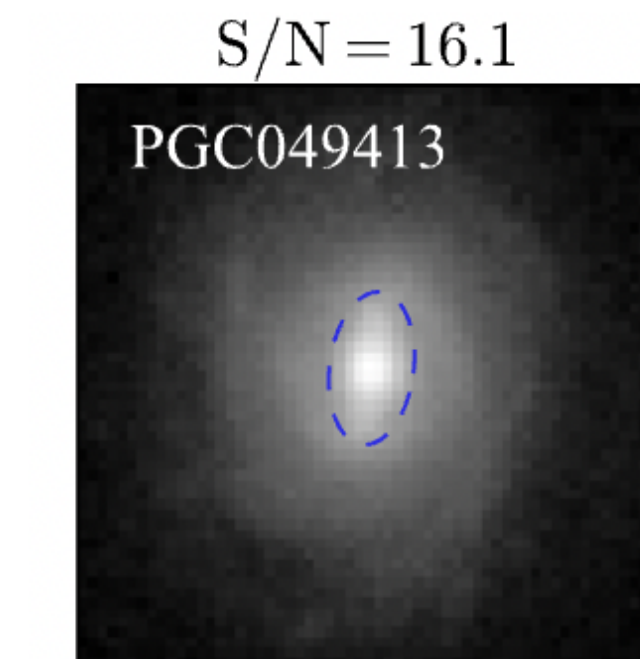
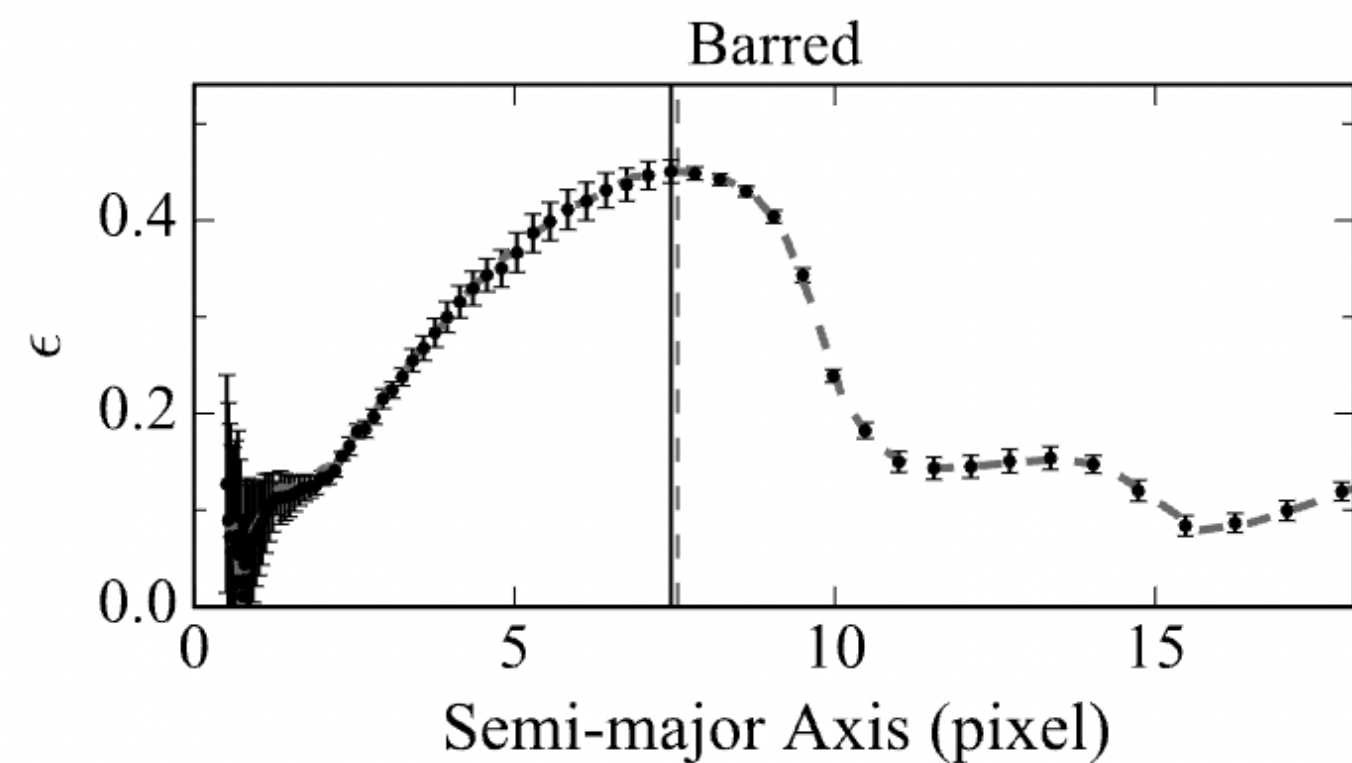
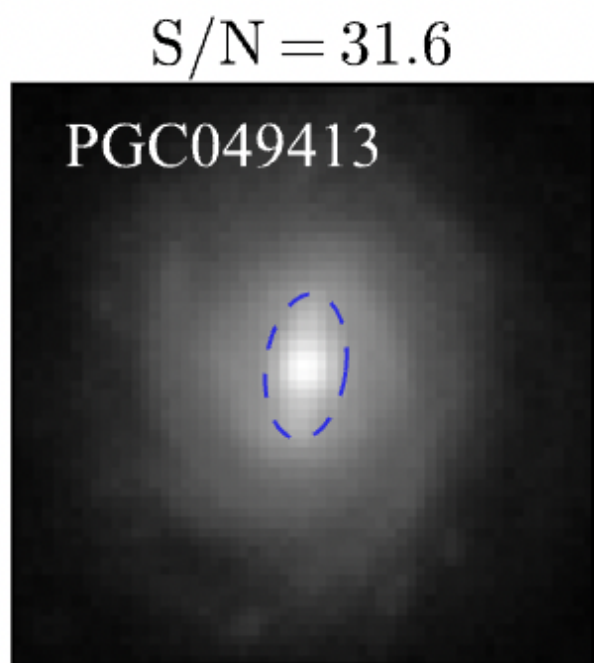
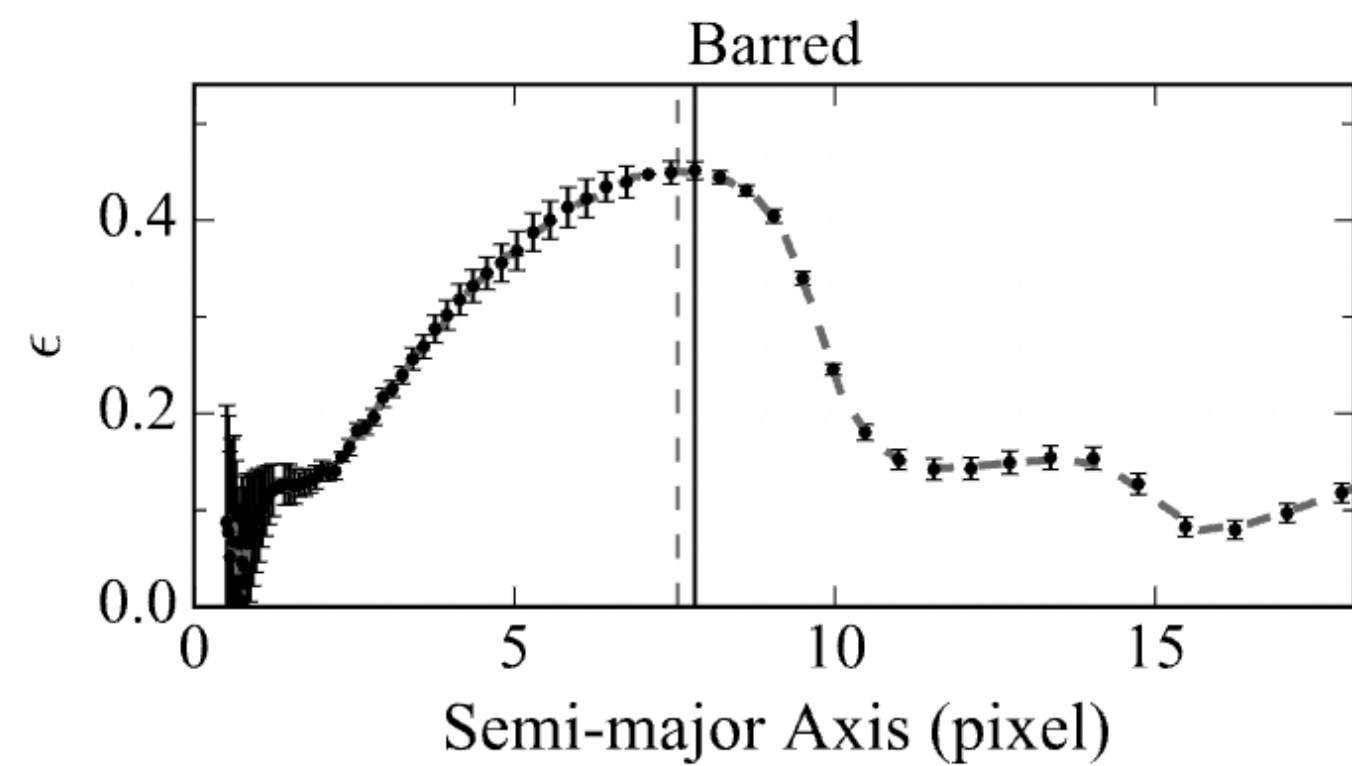
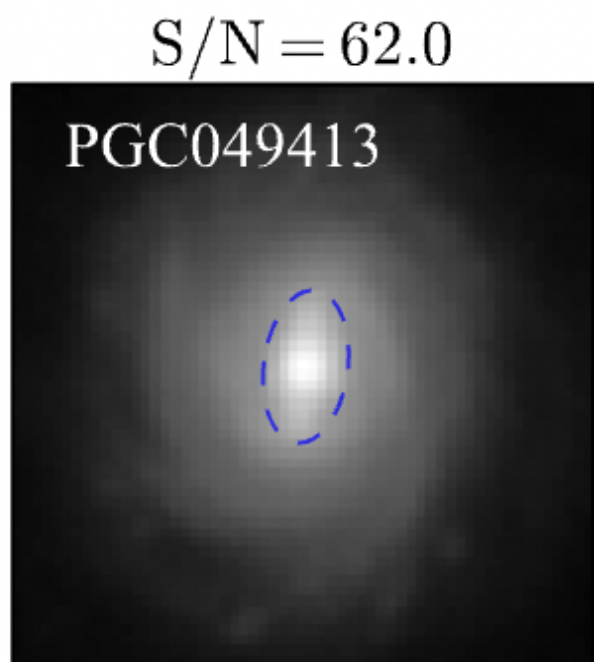
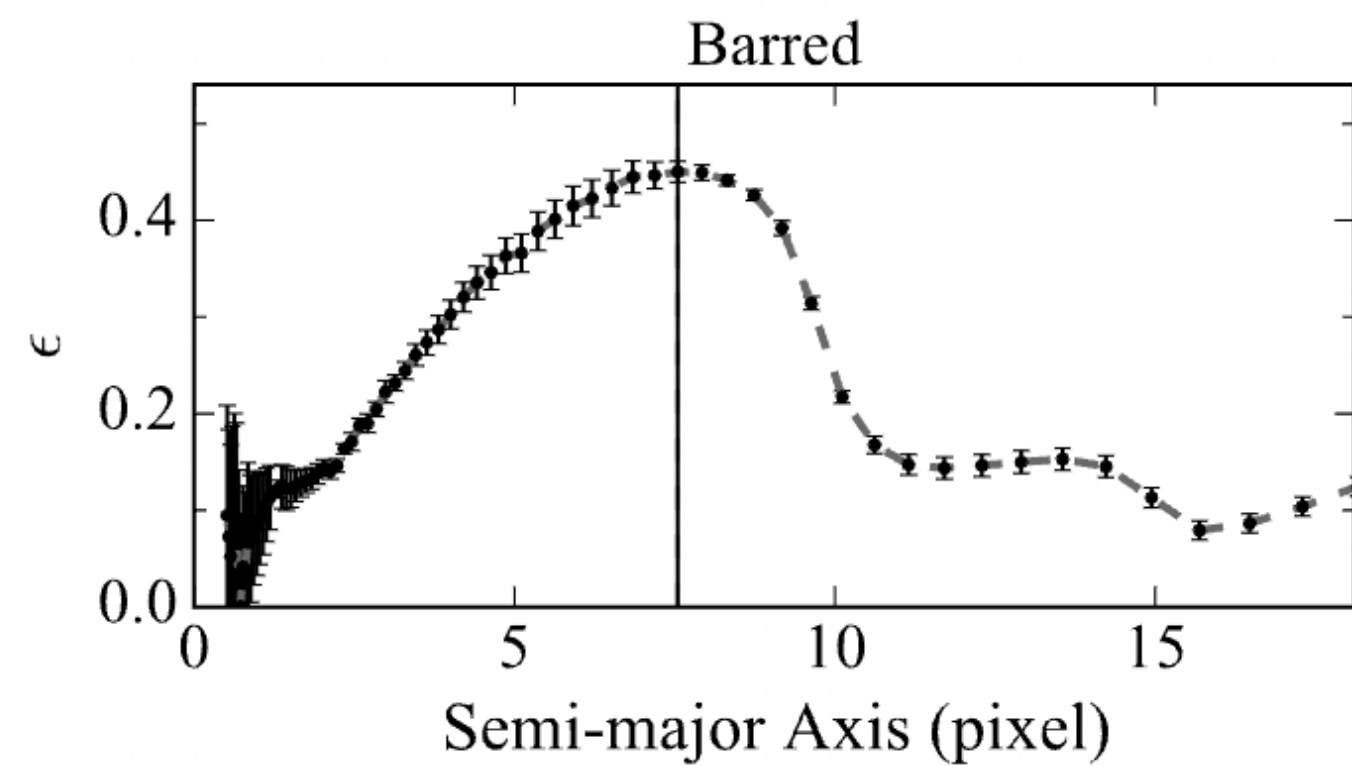
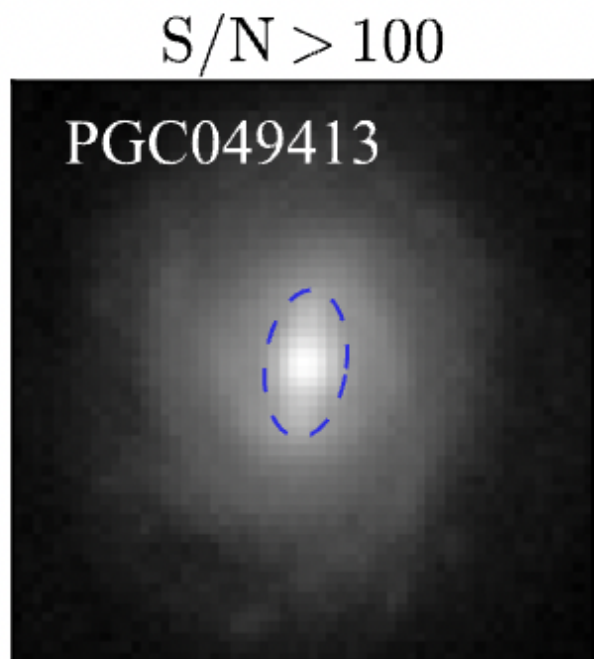
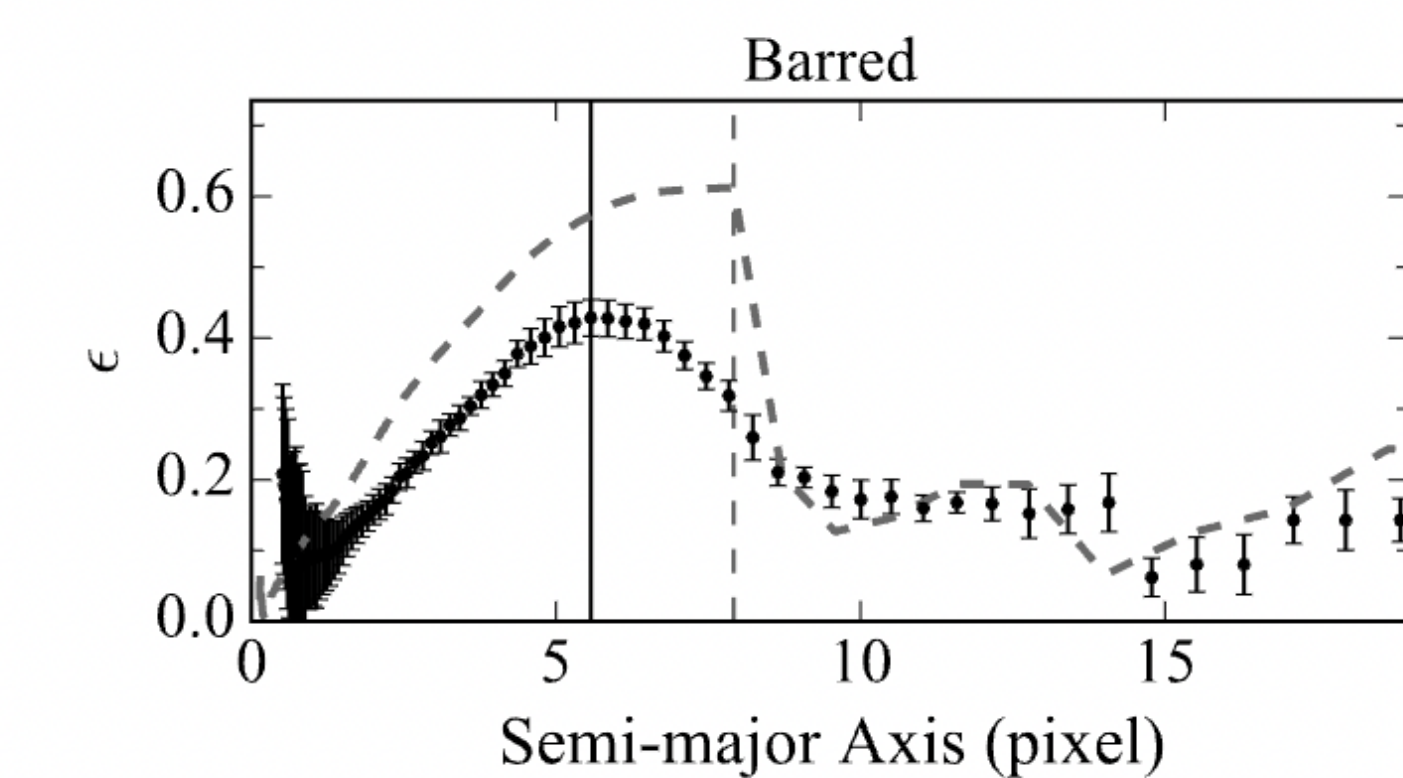
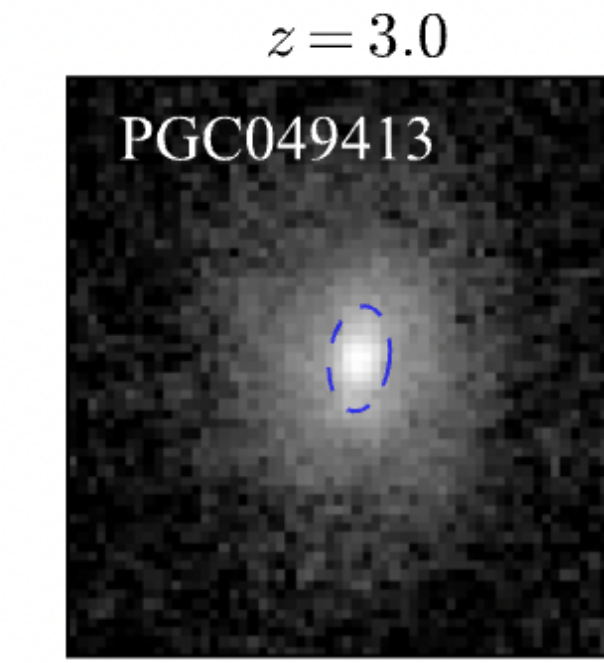
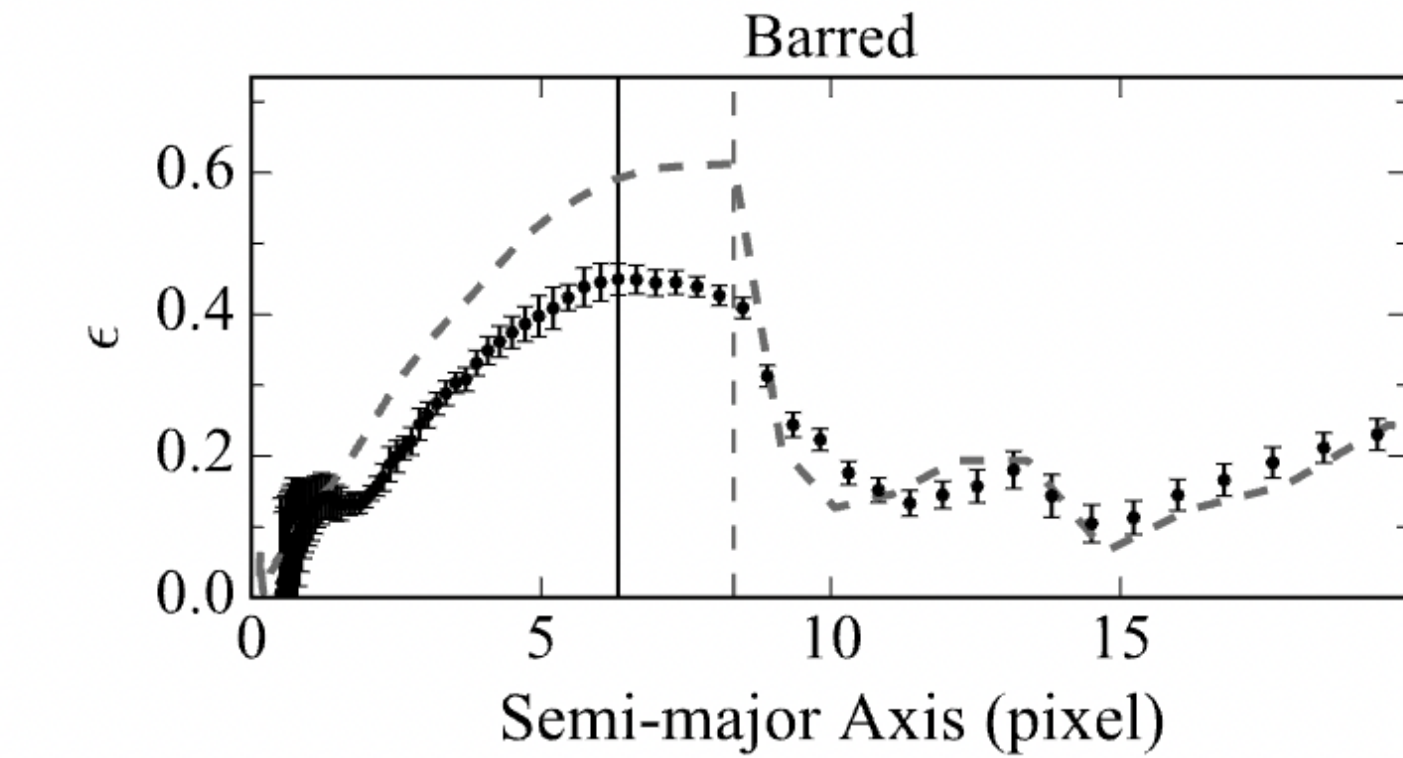
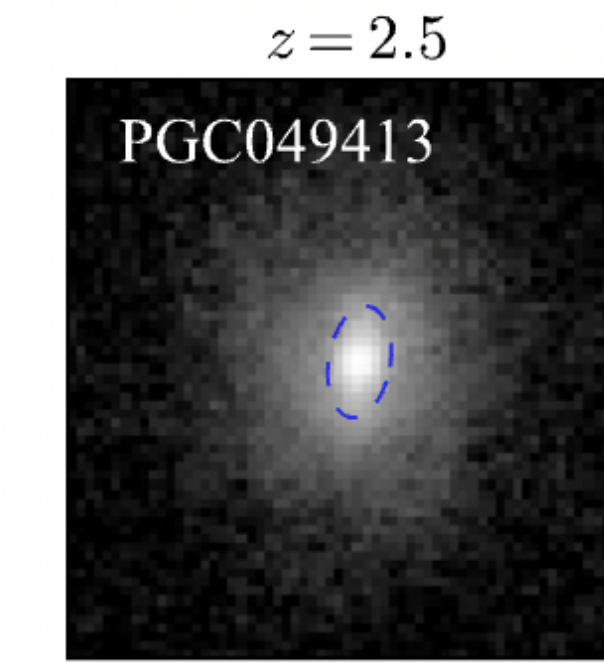
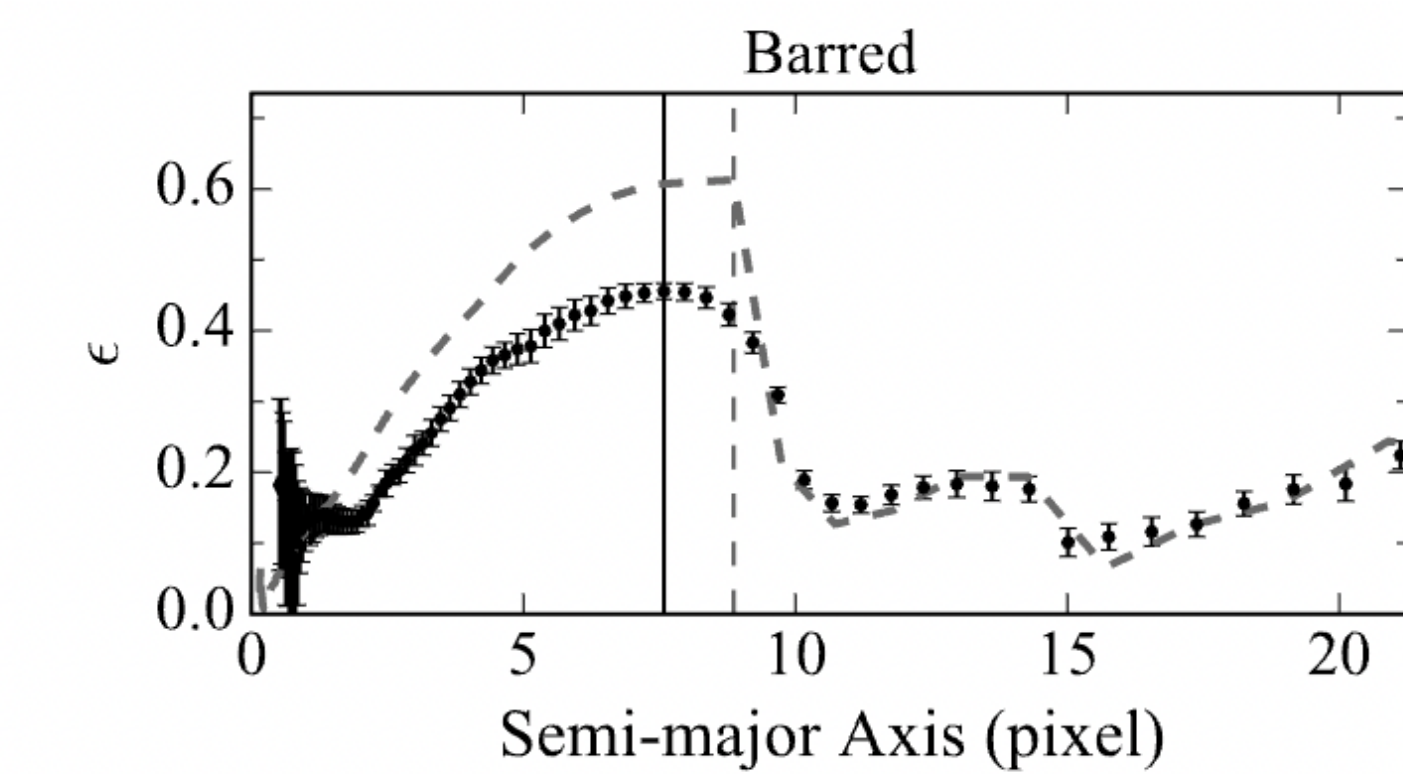
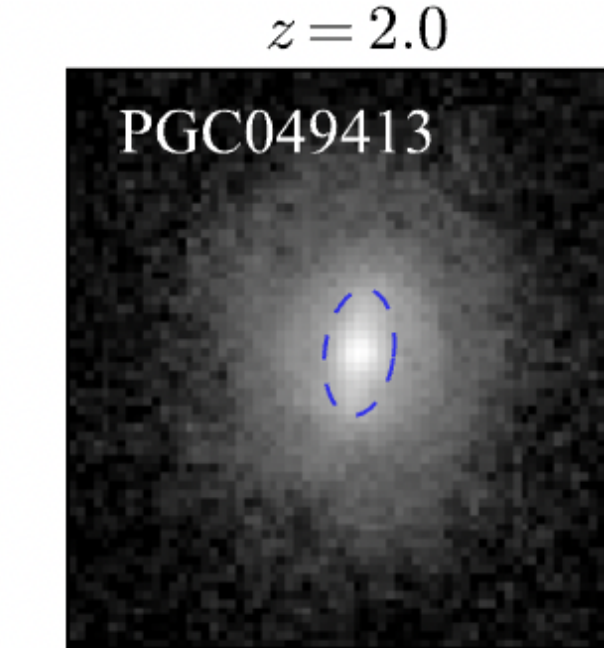
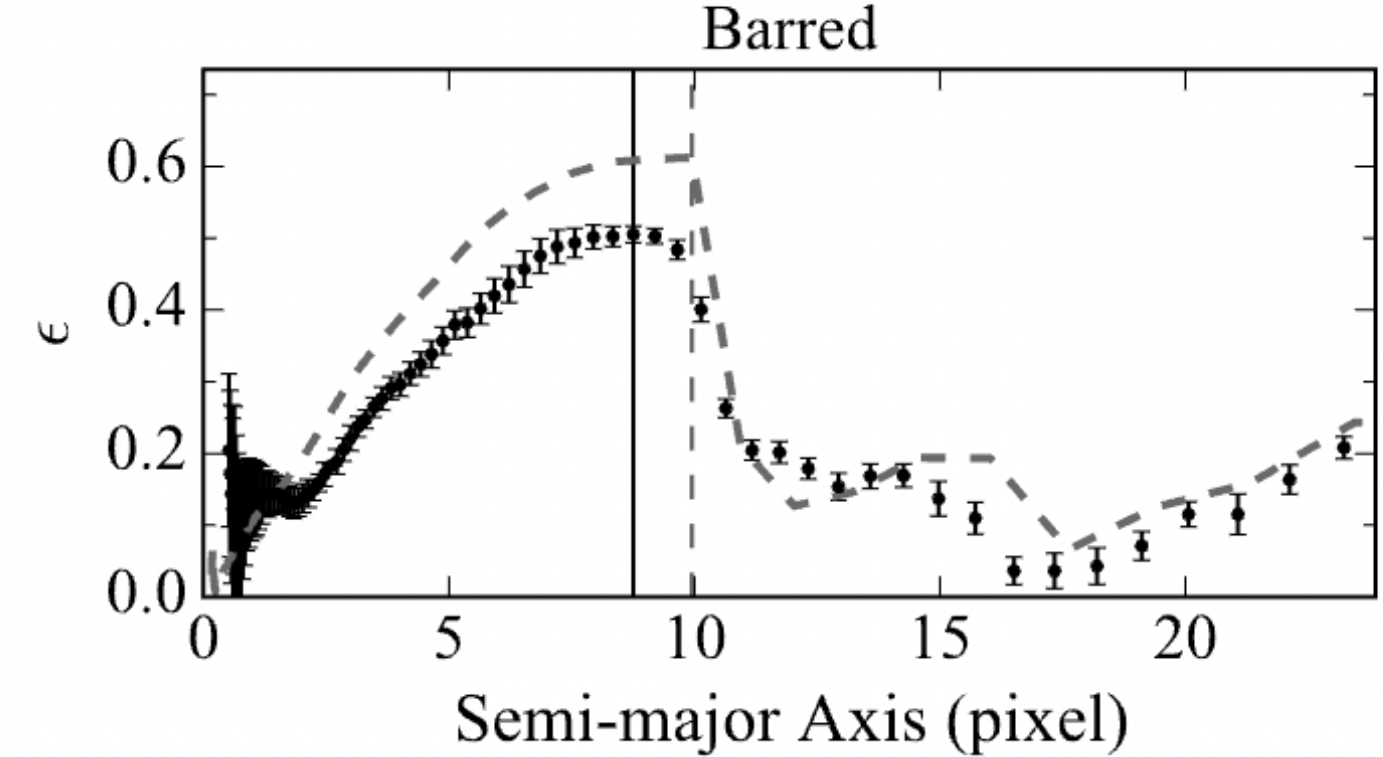
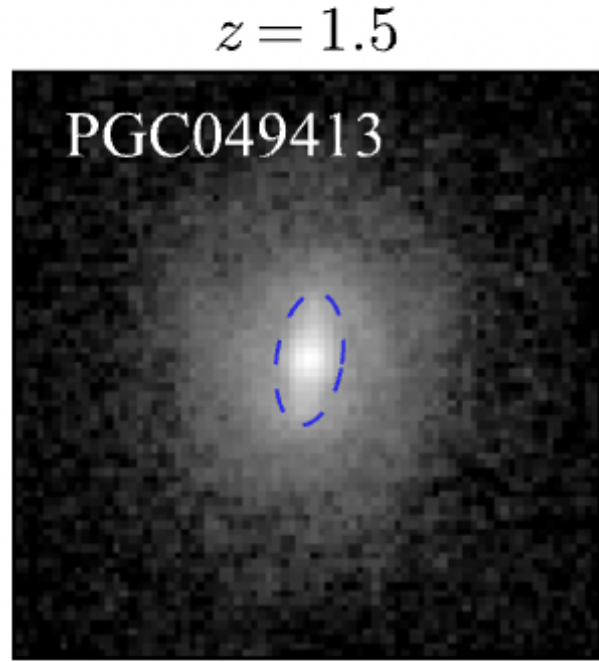
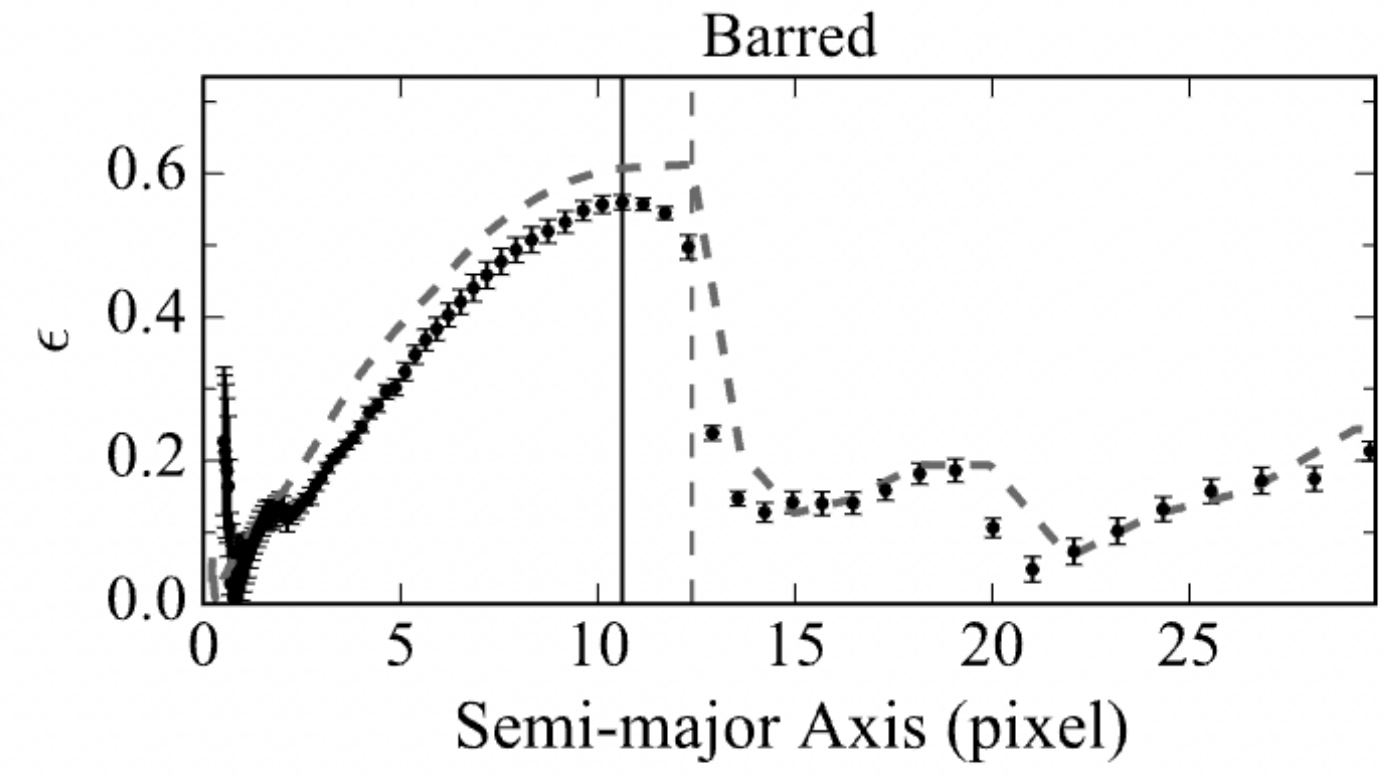
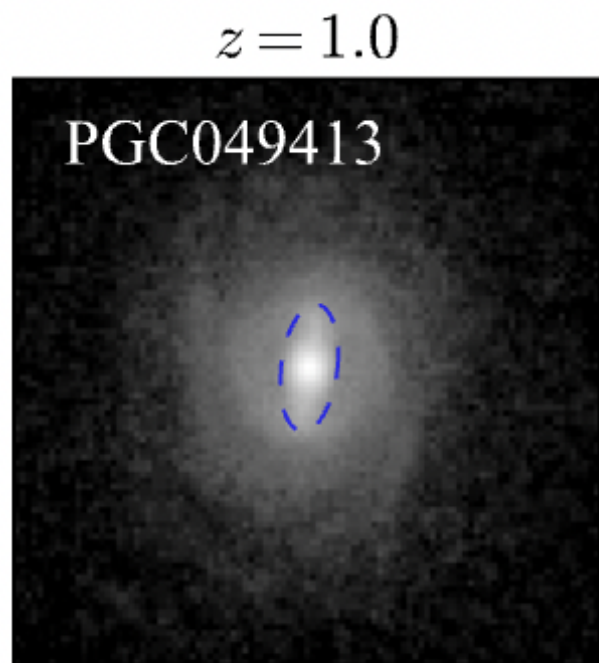
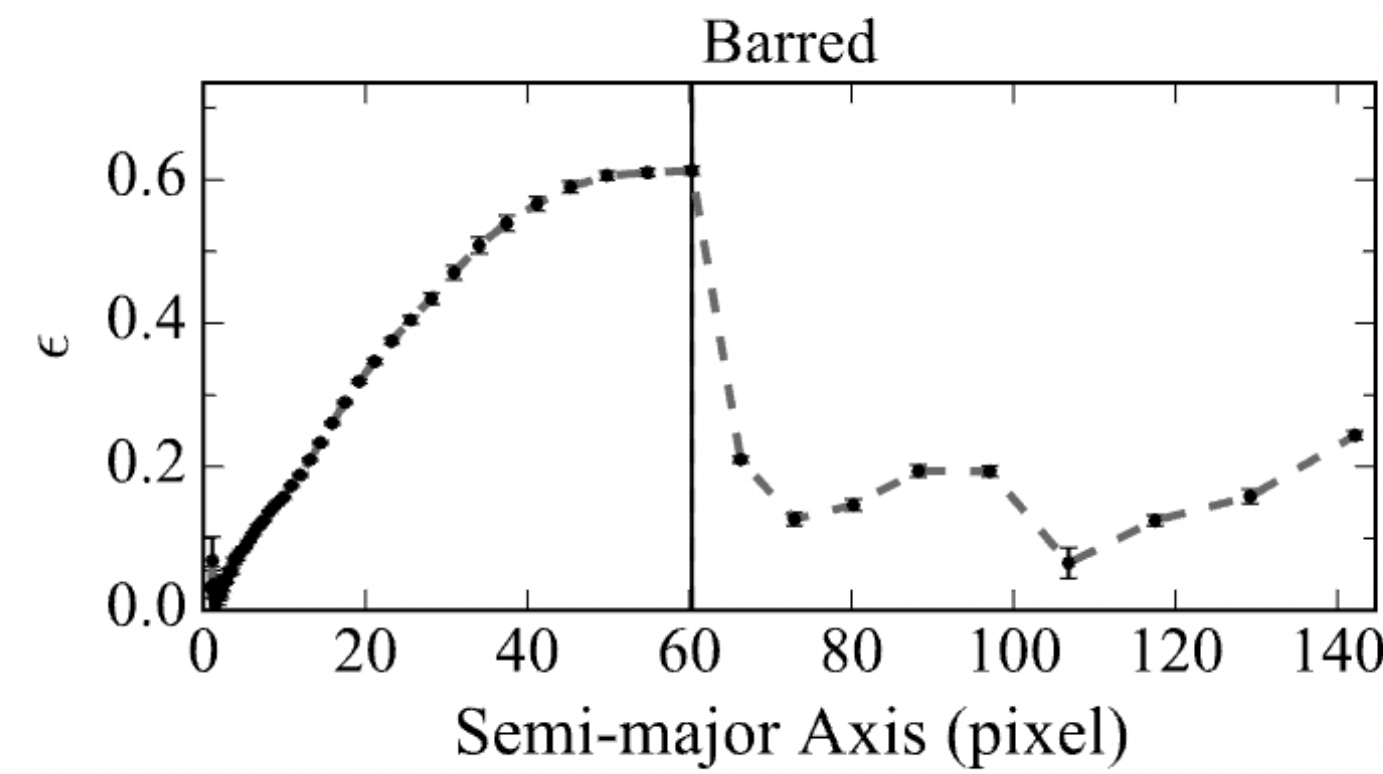
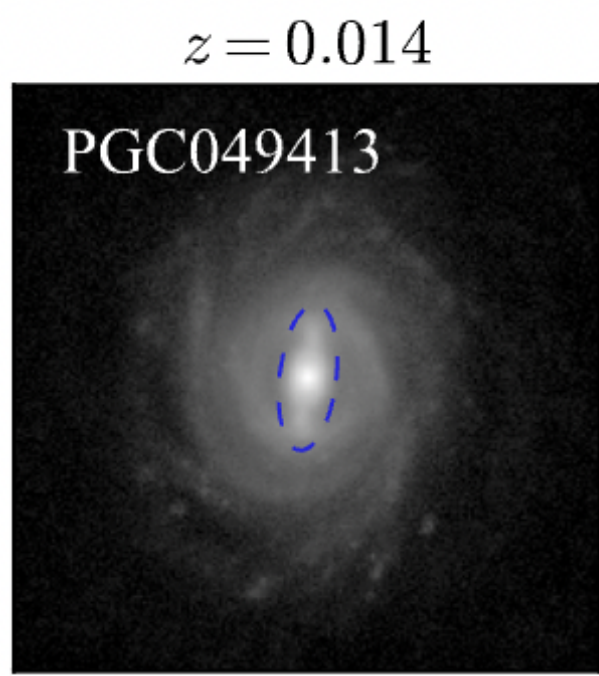


# Image simulations

## Simulated galaxy images observed in CEERS

- Yu et al. (2023) used a sample of nearby galaxies to generate artificially redshifted images observed with JWST CEERS.
- The dataset is perfectly match our scientific goal of understanding how the observational condition in CEERS affects the bar measurement.
- The properties measured from low-resolution images are denoted as  $\epsilon_z$ ,  $\alpha_z$  and  $\text{PA}_z$

# Simulated galaxy images observed in CEERS



# Measurement robustness of bar structures

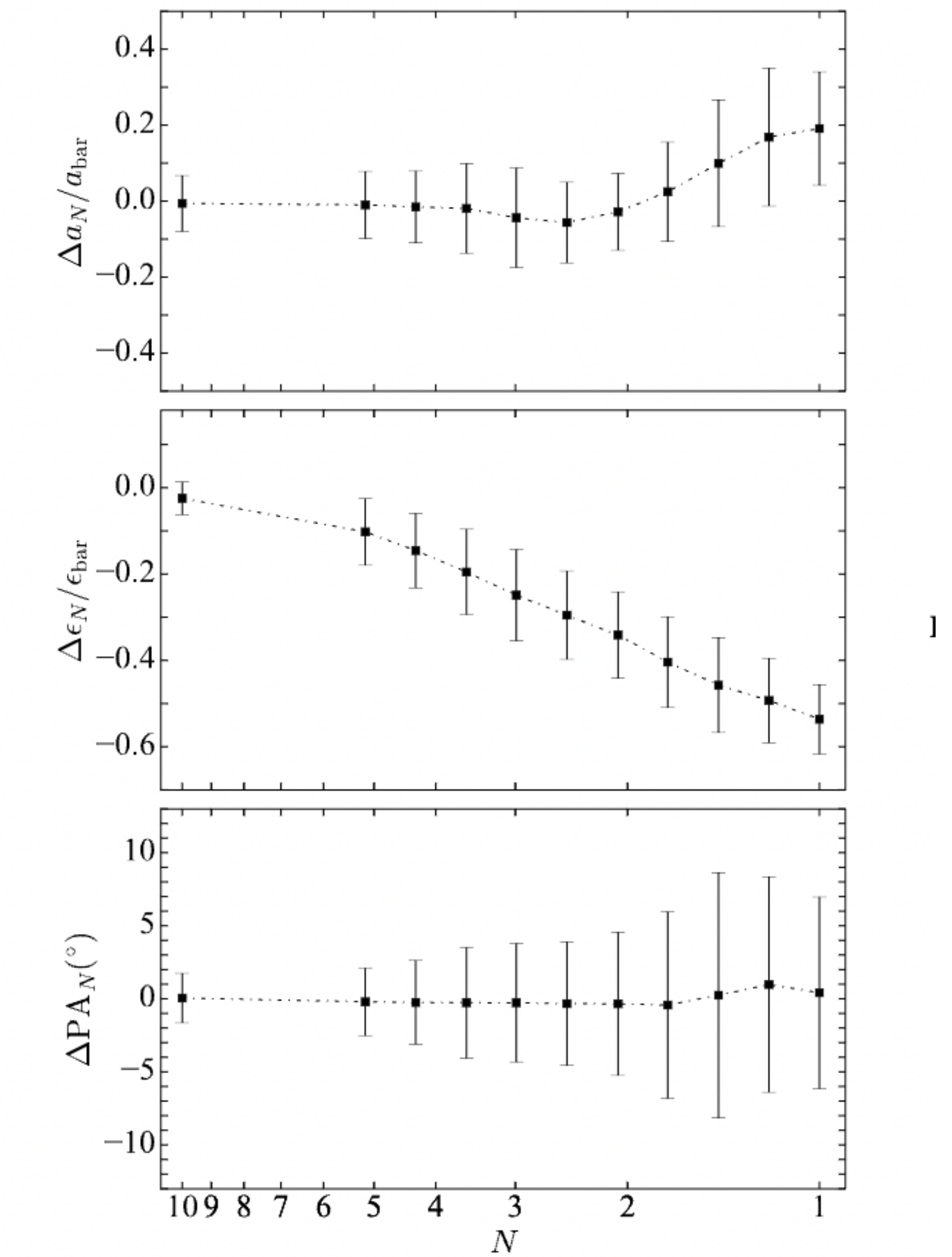
## The effect of resolution

- After  $N = 2.07$ , the  $a_N$  tend to be larger than  $a_{\text{bar}}$ .
- Due to the PSF smoothing effect, the  $\epsilon_N$  is progressively smaller than  $\epsilon_{\text{bar}}$  as the resolution decreases.
- The orientation of the bar is slightly affected by decreasing resolution.

$$\Delta a_N = (a_N - a_{\text{bar}})/a_{\text{bar}}$$

$$\Delta \epsilon_N = (\epsilon_N - \epsilon_{\text{bar}})/\epsilon_{\text{bar}}$$

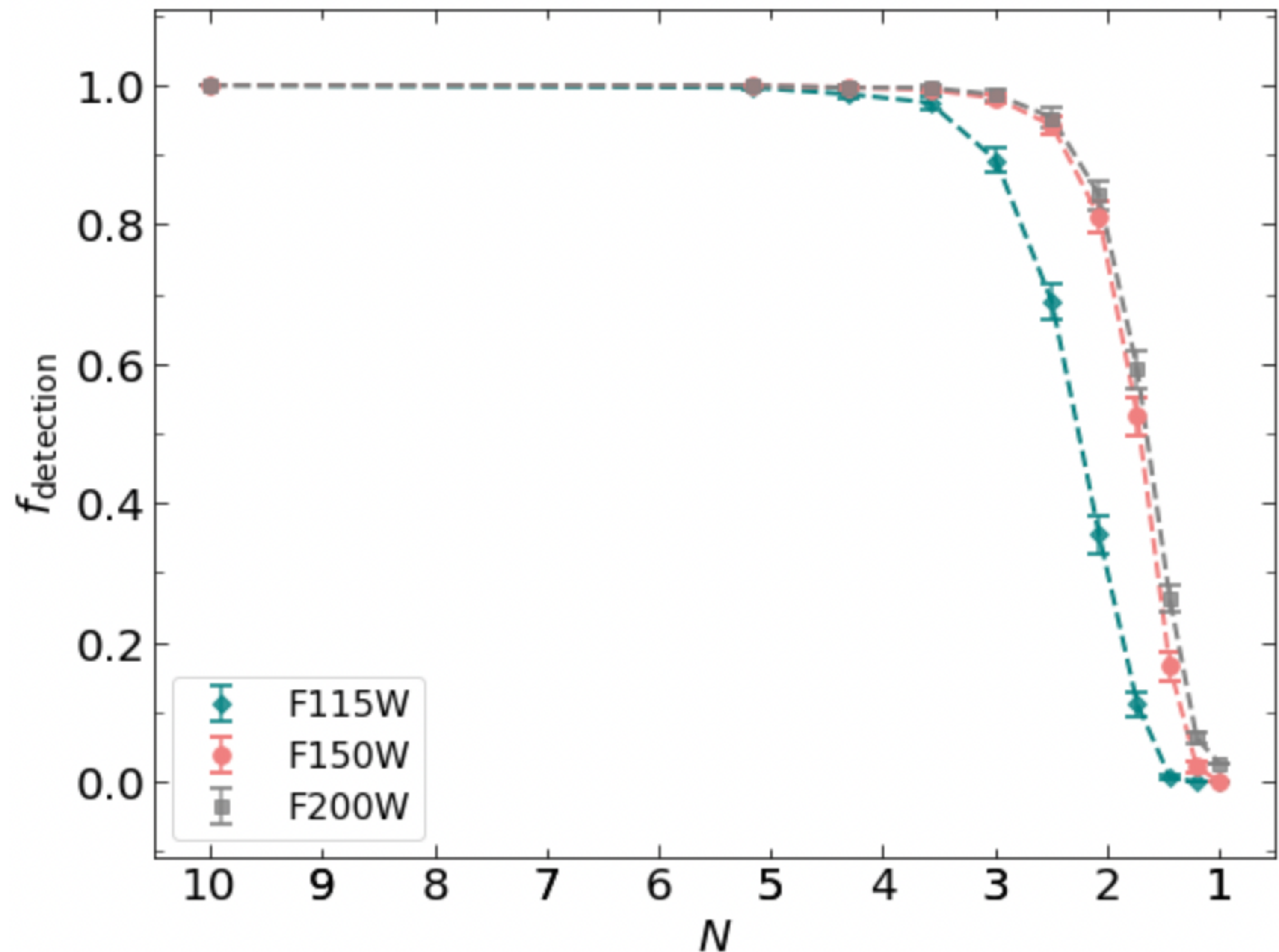
$$\Delta \text{PA}_N = (\text{PA}_N - \text{PA}_{\text{bar}})/\text{PA}_{\text{bar}}$$



# Measurement robustness of bar structures

## The effect of resolution

- In the case of F150W and F200W filters, the  $f_{\text{detection}}$  does not exhibit a sudden decline until reaching a resolution level approximately around  $N = 2$ .
- In the case of the F115W filter, the resolution level at approximately  $N = 3$  serves as a turning point for bar identification.



# Measurement robustness of bar structures

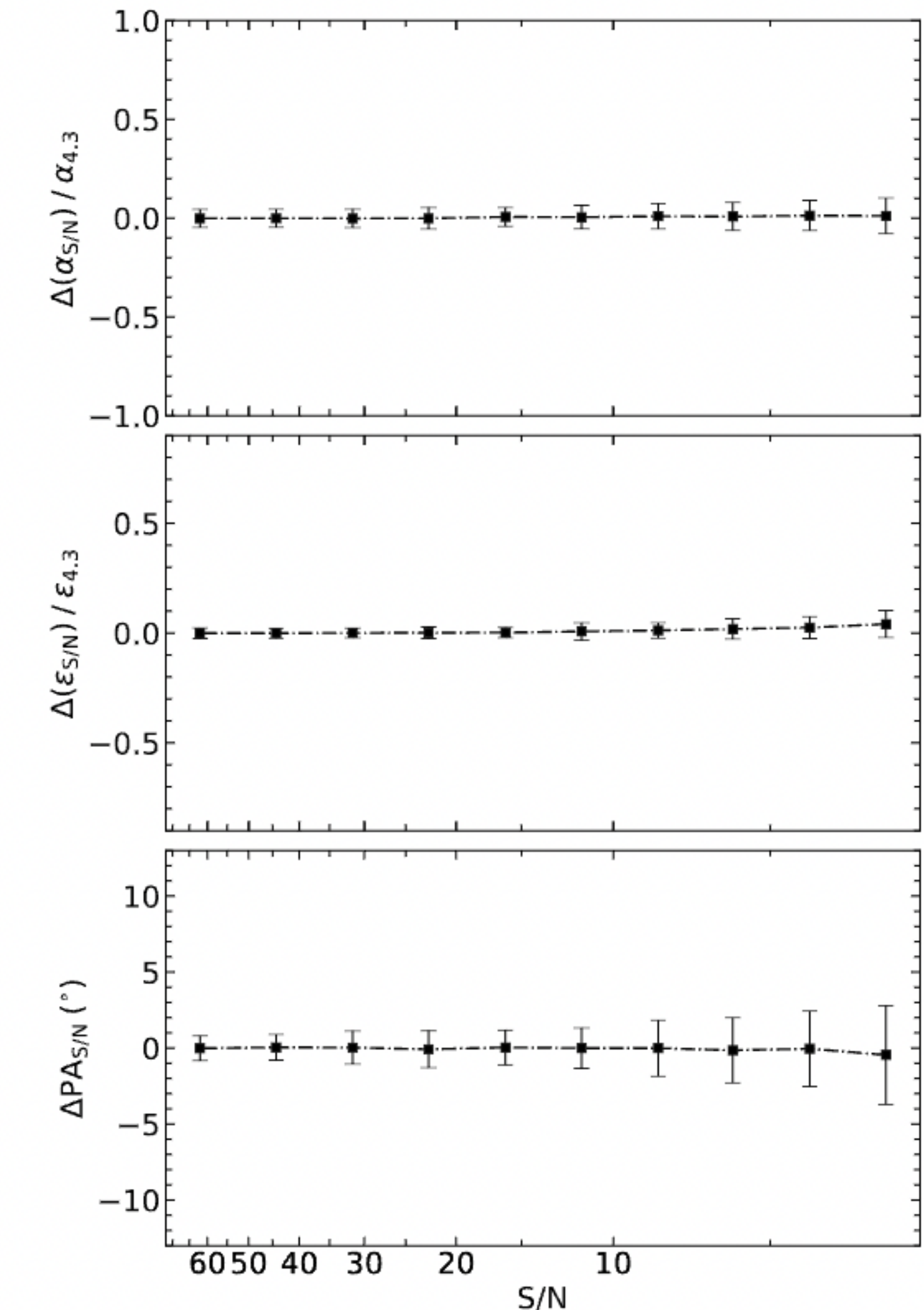
## The effect of noise

- The measurement of bar structures is slightly affected by the decreasing S/N within the typical S/N range of CEERS.

$$\Delta a_{S/N} = (a_{S/N} - a_{4.3})/a_{4.3}$$

$$\Delta \epsilon_{S/N} = (\epsilon_{S/N} - \epsilon_{4.3})/\epsilon_{4.3}$$

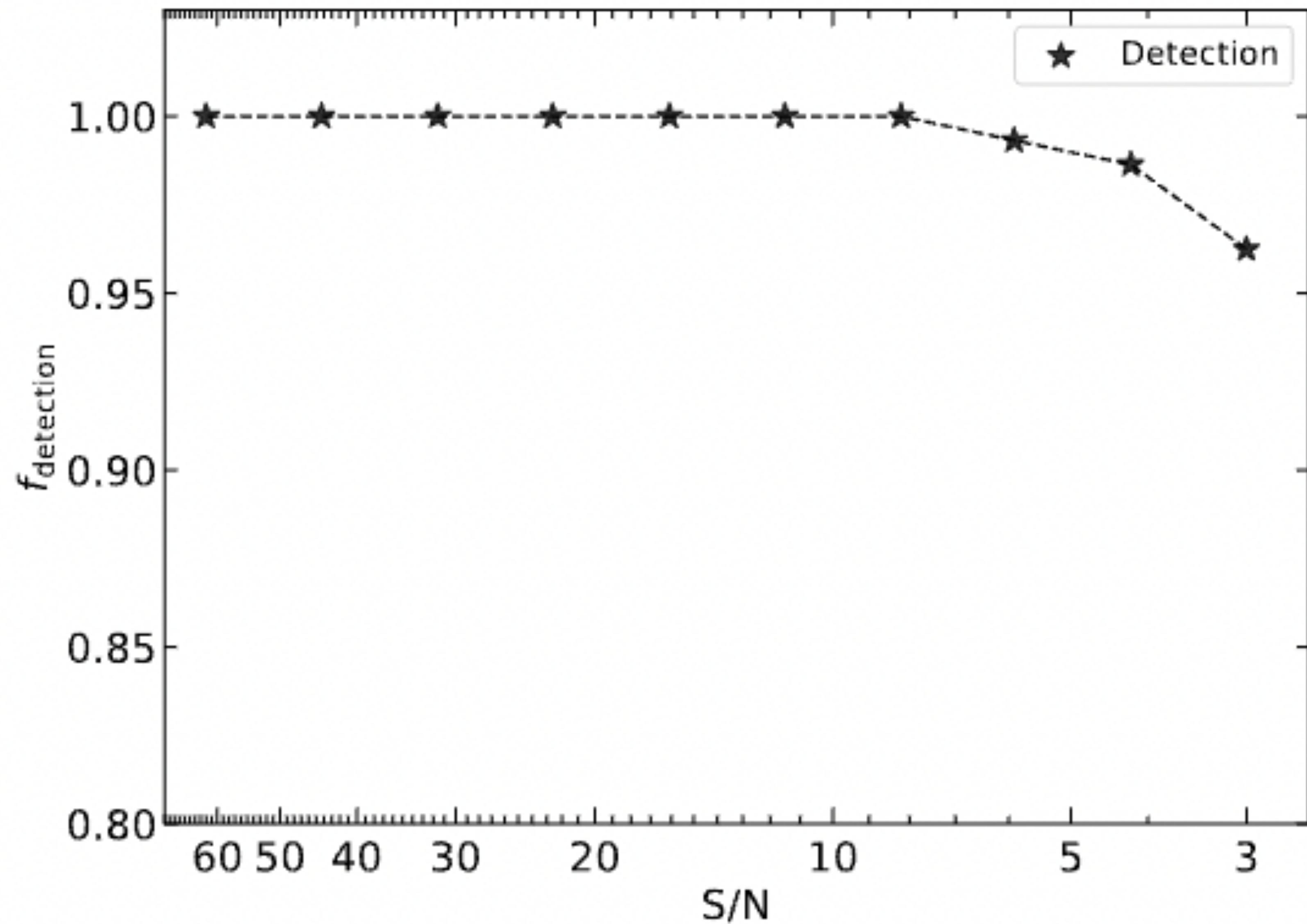
$$\Delta PA_{S/N} = (PA_{S/N} - PA_{4.3})/PA_{4.3}$$



# Measurement robustness of bar structures

## The effect of noise

- Handful fraction of bars can be lost as S/N level is lower than 10.



# Measurement robustness of bar structures

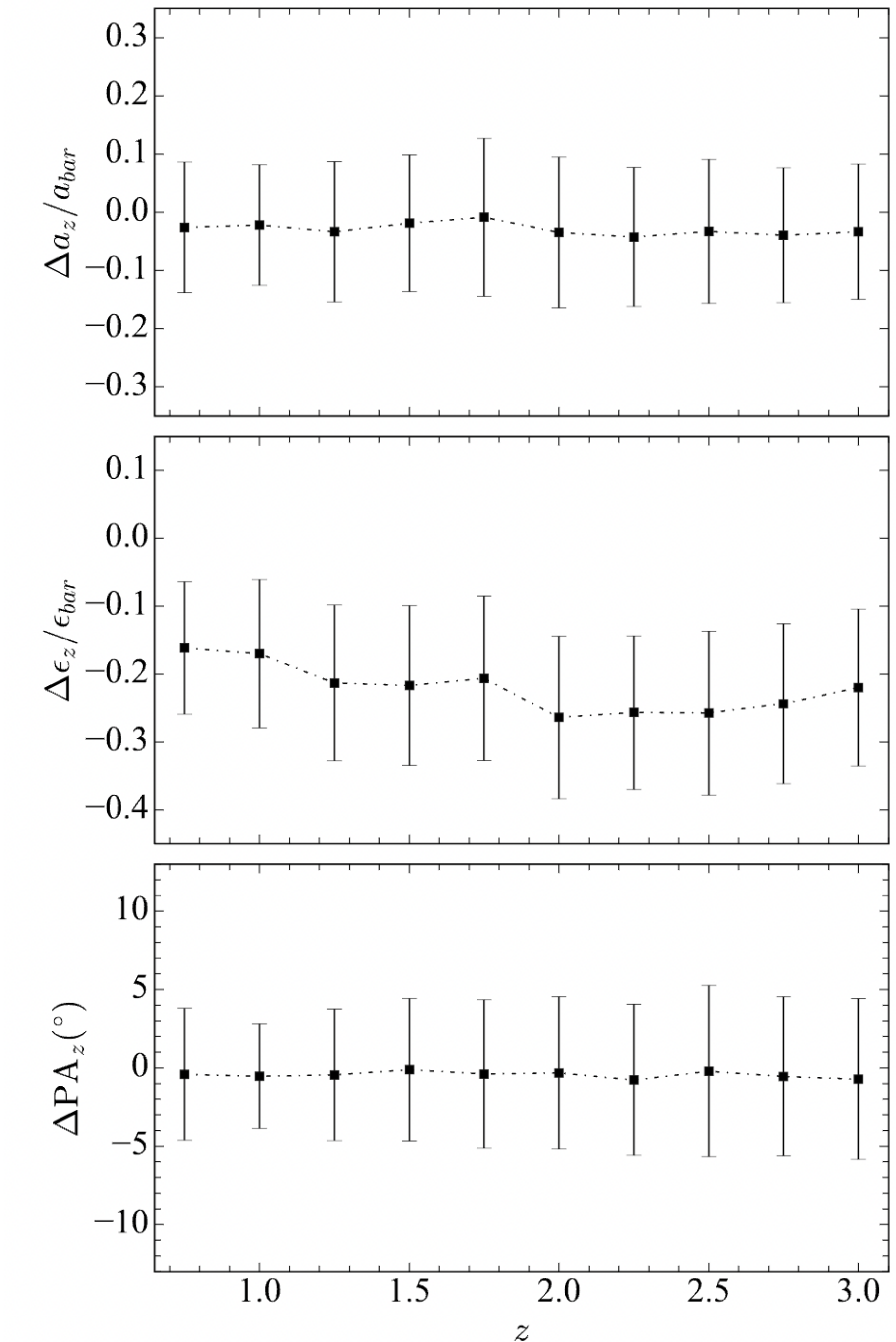
## Artificially redshifted images

- Primarily influenced by resolution effects, the  $\epsilon_z$  is consistently smaller than  $\epsilon_{\text{bar}}$ , while the  $a_z$  remains relatively consistent with the  $a_{\text{bar}}$ .

$$\Delta a_z = (a_z - a_{\text{bar}})/a_{\text{bar}}$$

$$\Delta \epsilon_z = (\epsilon_z - \epsilon_{\text{bar}})/\epsilon_{\text{bar}}$$

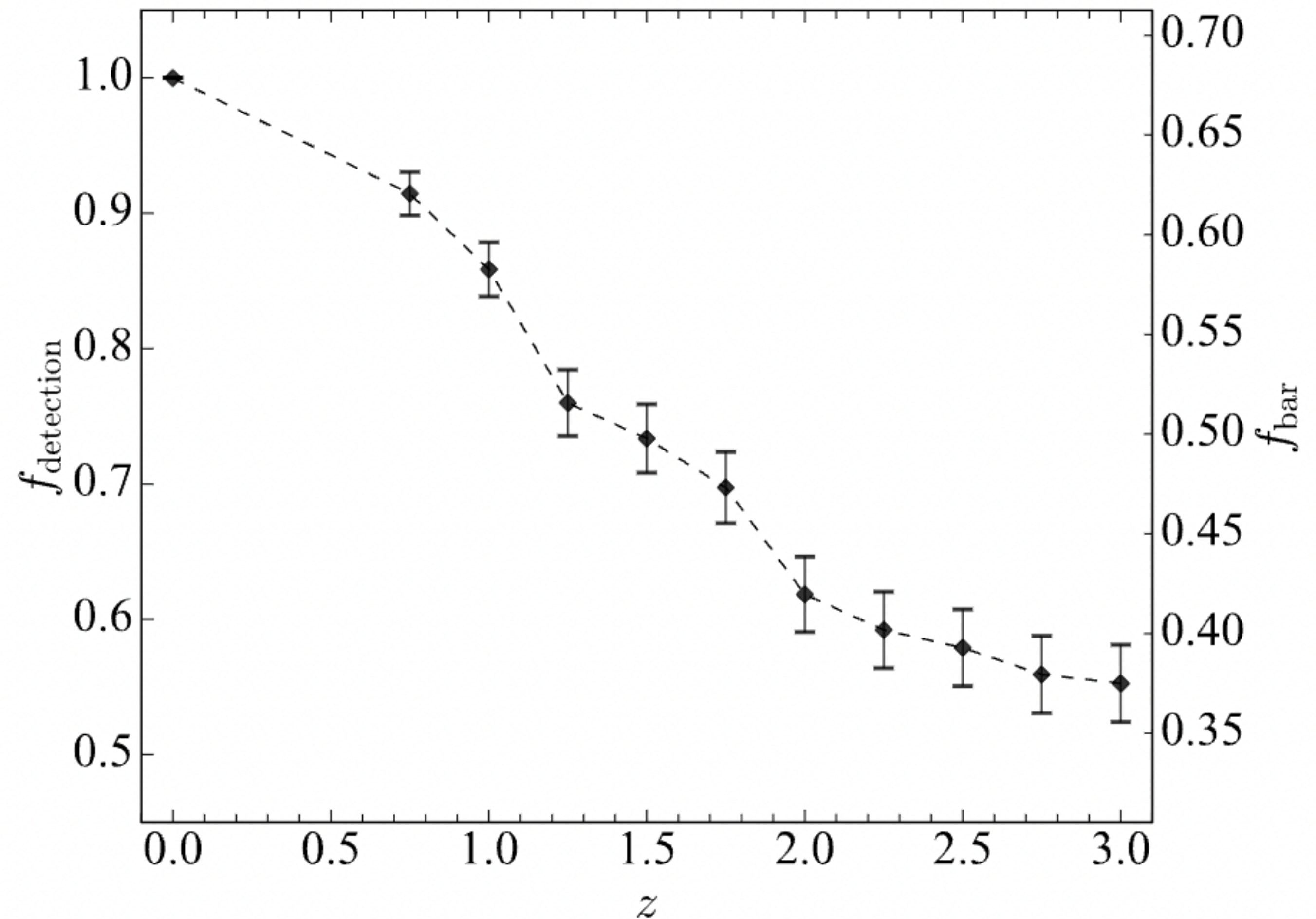
$$\Delta \text{PA}_z = (\text{PA}_z - \text{PA}_{\text{bar}})/\text{PA}_{\text{bar}}$$



# Measurement robustness of bar structures

Artificially redshifted images

- Numbers of bars can be undetected at higher redshifts, around half of bars can go undetected at  $z=3$ .



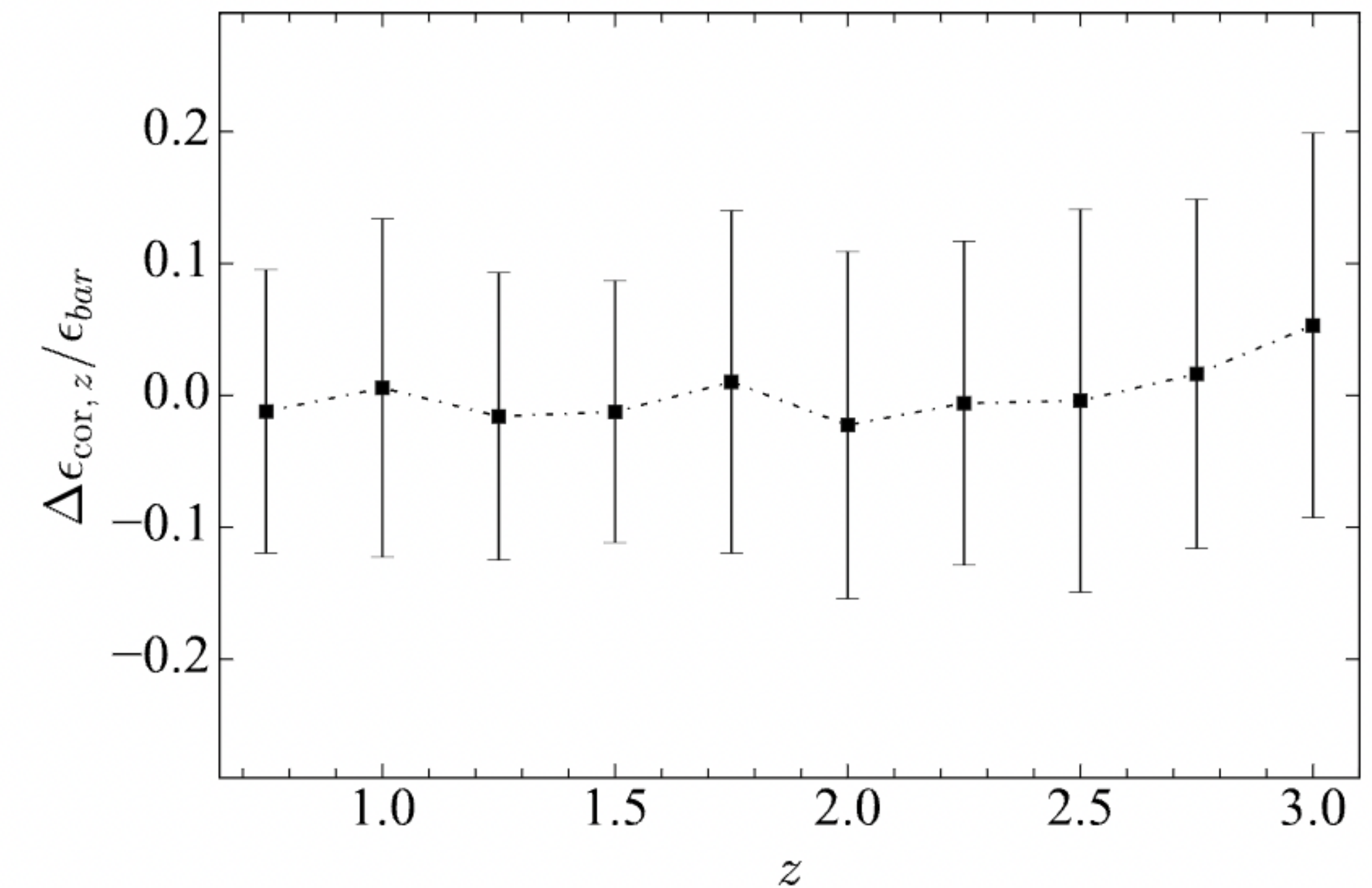
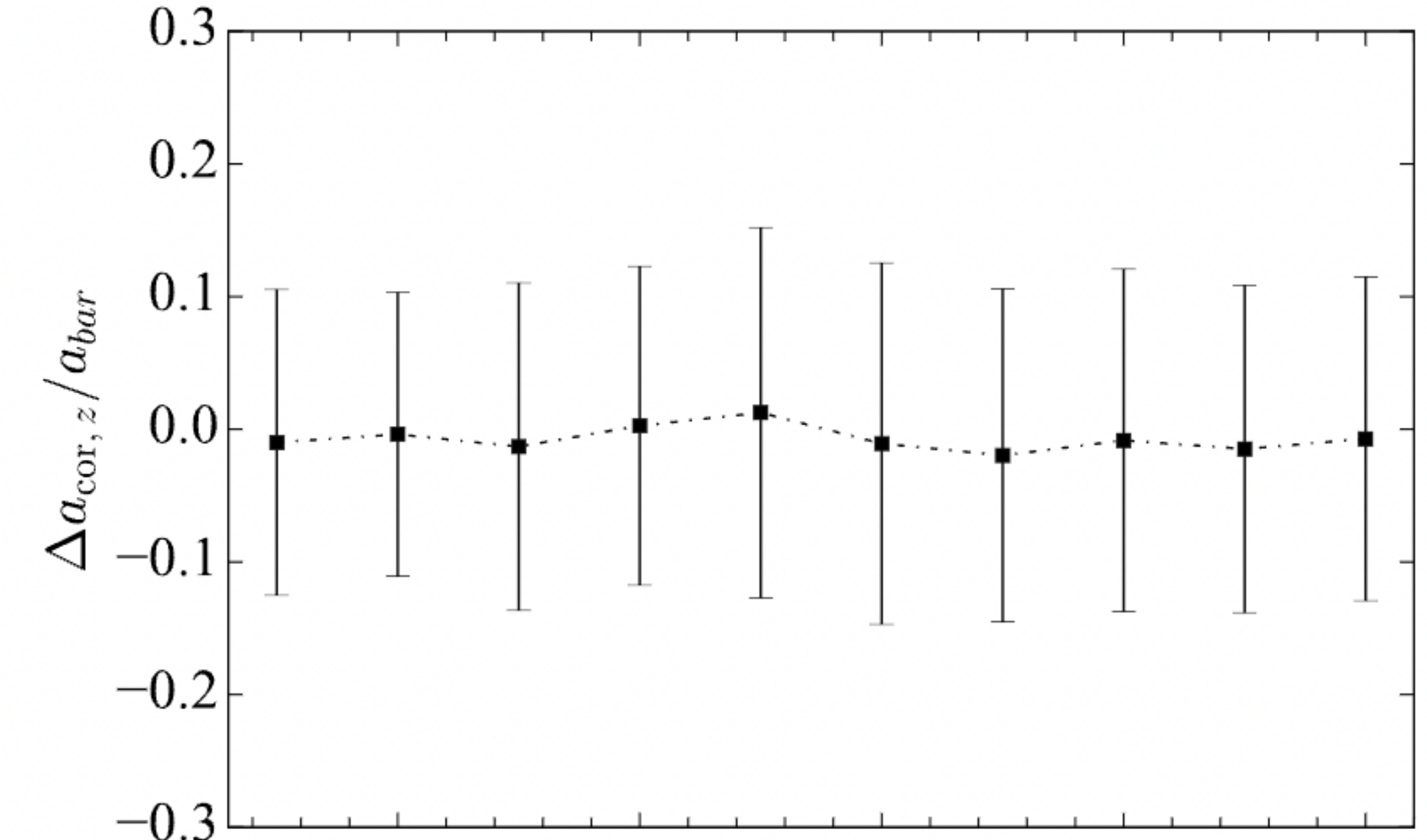
# Measurement robustness of bar structures

**Bias corrected**

- After bias correction, the parameters  $a_{\text{cor}, z}$  and  $\epsilon_{\text{cor}, z}$  closely align with their intrinsic values.

$$a_{\text{cor}, z} = \frac{a_z}{(\Delta a_N/a + 1)}$$

$$\epsilon_{\text{cor}, z} = \frac{\epsilon_z}{(\Delta \epsilon_N/\epsilon + 1)}.$$



# Summary

- We start from a sample of 448 low-redshift galaxies from DESI, a subset of the sample conducted by Yu et al. 2023.
- The galaxies are initially classified into barred and unbarred categories using the ellipse fitting method, and their bar properties ( $a_{\text{bar}}$ ,  $\epsilon_{\text{bar}}$ , and  $\text{PA}_{\text{bar}}$ ) are measured. Next, we use the barred galaxies to simulate low-resolution and low S/N images. Meanwhile, we also take advantage of the simulated CEERS images generated by Yu et al. 2023.
- In all three categories of simulated images, we re-identify bars and re-measure their properties.
- The measurement of  $a_{\text{bar}}$  and  $\epsilon_{\text{bar}}$  can be significantly influenced by the resolution, while  $\text{PA}_{\text{bar}}$  is only slightly affected
- For the F150W and F200W low-resolution images, with Nyquist-sampling PSFs, the limit of bar detection occurs at approximately  $N \sim 2$ . For the F115W low-resolution images, the turning point appears around  $N \sim 3$ .

# Summary

- Our findings indicate that within this typical S/N range of typical S/N range for galaxies within the redshift range  $0.75 \leq z \leq 3.0$  and stellar mass  $M_\star \geq 10^{9.75} M_\odot$ , both the identification and measurements of bars are minimally affected by noise.
- Using the simulated CEERS images, we find a decrease in the bar fraction (detection rate) from 68% (100%) in the local Universe to 37.5% (55%) at redshift  $z=3.0$ . This decrease is attributed to the effects of resolution degradation, galaxy angular size changes due to distance, and intrinsic evolution.
- We find that the  $a_{\text{bar}}$  measured from the simulated CEERS images tends to be slightly underestimated, with the fractional difference remaining below 0.1. Additionally, we found that the  $\epsilon_{\text{bar}}$  measured from the simulations is significantly underestimated, and this underestimation exhibits a minor trend of increasing with higher redshift.
- The bias correction functions are developed using results from the low-resolution images, after bias correction, the parameters are closely align with their intrinsic values